NANOSECOND PULSE RADIOLYSIS STUDIES

by

GERALDINE ANNE KENNEY

Licentiate of the Royal Institute of Chemistry, London

1965

A THESIS SUBMITTED IN PARTIAL FULFILMENT OF

THE REQUIREMENTS FOR THE DEGREE

MASTER OF SCIENCE

in the Department

of

Chemistry

We accept this thesis as conforming to the

required standard.

THE UNIVERSITY OF BRITISH COLUMBIA

April, 1968

Department of Chemistry
The University of British Columbia
Vancouver 8, B.C., Canada
April 16, 1968

Abstract

Nanosecond pulse radiolysis studies on the behaviour of $\bar{e}$ aq at high concentrations as a preliminary to the investigation of $\bar{e}$ aq* have shown that contrary to normal classical homogeneous kinetics the electron decays initially in a first order manner, moving into second order decay within about 100 nanoseconds after the electron pulse. Further investigations have shown that for a comparable time after the pulse the distribution of the absorbing species is not homogeneous thus rendering any classical kinetic interpretation invalid. Qualitative calculations on the duration of the inhomogeneity were performed and the experimental results are in reasonable agreement with their predictions.

The first order decay that is observed is considered to be more than a random sequence of reactions and two possible models are tentatively proposed to account for these events.

Comparisons are made between this work and others in which inhomogeneity undoubtedly accounts for the unusually fast bimolecular rate constants for the primary decay

$$\bar{e} \text{ aq} + \bar{e} \text{ aq} \longrightarrow H_2 + 2OH^- \text{ aq}$$
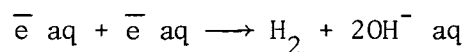
The deuterated electron was investigated with similar conclusions.

The rate constants evaluated from this work were:

$\bar{e}$ aq $\qquad k_1 = 8.80 \pm .80 \times 10^6 \text{ sec}^{-1}$

$\qquad\qquad k_2 = 5.88 \pm 1.20 \times 10^{10} \text{ M}^{-1} \text{ sec}^{-1}$

$\bar{e}$ d $\qquad k_1 = 8.14 \pm .21 \times 10^6 \text{ sec}^{-1}$

$\qquad\qquad k_2 = \sim 10^{11} \text{ M}^{-1} \text{ sec}^{-1}$

and the bimolecular rate constant, determined in a homogeneous environment, is in good agreement with the accepted literature values for the probable reactions involving $\overline{e}$ aq in our system.

Table of Contents

List of Tables

List of Illustrations

The assistance of Mr. D.A. Head is acknowledged in Diagrams 1, 2 and 20.

Acknowledgment

I would like to thank Dr. D.C. Walker for his valued advice, patience and encouragement during the course of this research and in the preparation of this thesis.

Interactions of Ionising Radiation with Matter

The absorption of high energy radiations of either particle or
electromagnetic origin induces ionisation, excitation and a series of
physicochemical processes all of which occur in the absorbing target
material. Radicals, ions and excited species produced as a consequence
of these primary effects then interact with their molecular environment
and give rise to the stable chemical products. Although termed "ionising"
these radiations are not necessarily restricted to ionising behaviour
as will become clear during this introductory section. Some of the aspects
of the physical consequences of the interactions of radiation and matter
will be discussed as a basis for the chemical reactions that ultimately
occur.

The energy of a ray or particle can be wholly or in part
transferred to the medium through which the radiation is passing. The
mechanisms by which energy is transferred to, and then dissipated in
the medium are to some extent characteristic of the incident radiation,
and to some extent dependent on the material itself. For electromagnetic
radiations which will now be discussed there are three main processes,
each of which may dominate under specified circumstances.

Electromagnetic radiation

As a photon impinges on the surface of a target material there
may be a transfer of energy resulting in a change of direction and energy
of the incident photon; alternatively there may be simply a reduction
in the intensity of the transmitted radiation in accordance with

$$\Delta I = -\mu I \Delta x$$

where x is the thickness of the absorbing material, ΔI the loss of intensity and μ the linear absorption coefficient. For a non-monoenergetic beam of photons incident on the material

$$I = I_1 e^{-\mu_1 x} + I_2 e^{-\mu_2 x} + I_j e^{-\mu_j x}$$

where (I_j, μ_j) characterises a photon of energy E_j.

The three important interactions to consider are

(i)   the photoelectric effect

(ii)   the Compton effect

(iii)   pair production

and of these only one under any given set of conditions will contribute significantly to the energy exchange processes.

(i)   The photoelectric effect describes the absorption of photons of low energy, 1 KeV < E_j < 500 KeV, by materials of high atomic number, Z, which results in the simultaneous angular ejection of a photoelectron whose energy is given by

$$E_{pe} = E_j - \phi$$

In metals ϕ is the work function, for other media ϕ is generally thought of as the binding energy but in either case may be equal to or more than the ionisation potential of the medium. The photoelectrons tend to be ejected at angles approaching 90° as the energy of the photon decreases. The sharp discontinuities observed on a graphical plot of photon energies versus atomic absorption coefficients related to the binding energy of the electrons in the different shells. Vacancies in the inner shells arising from a photoelectric process will be filled by outer shell electrons; energy is conserved with the emission of X-rays or low-energy auger electrons.

Coherent scattering of the incident photon by the atomic electrons increases as the electron density of the material increases and is generally most pronounced at low photon energies. This scattering occurs in the same energy regions as the photoelectric effect but is by comparison a weak interaction.

(ii) The Compton effect describes partially elastic collision of a photon with an electron during which the photon is scattered with a diminished energy E and the electron recoils with an increase in energy

$$E_r = E_j - E$$

As the scattering is angular the absolute value of the recoil energy E_r is a function of the angular relationship between the incident and scattered photons, and the accelerated electron.

$$E = \frac{Eo}{(1 + Eo/m_o c^2)(1 - \cos \theta)}$$

Er has values of zero (Er $\equiv$ Eo) and the maximum energy is given by letting $\theta \to 180°$

$$Er_{max} = \{ \frac{Eo}{1 + 0.25/Eo} \}$$

The Compton effect dominates radiation interactions between incident photons of several MeV and materials of high electron density, and photons of lower incident energies (20 KeV $< E_j <$ 2MeV) for materials of lower electron density. In a medium such as water Compton effects have been observed over the range 30 KeV $< E_j <$ 20 MeV.

(iii) pair production refers to the appearance of a positron and electron at the disappearance of the incident photon (in the vicinity of the atomic nucleus) whose energy is converted into the kinetic energy

and rest mass of these two particles. Photons of energy less than 1.02 MeV cannot participate in this process as the relationship

$$Ep + E_e = E_j - 2mc^2$$

must be satisfied. Following the formation of the pair the positron combines with an electron and two 0.51 MeV γ-rays are simultaneously emitted. These are referred to as annihilation radiation.

Summary

The atomic cross sections (or absorption coefficients) for all these processes increase with increasing electron density of the material involved. In a given medium and at low photon energies the most important effect is the photoelectric phenomenon; at medium photon energies the Compton effect dominates any other processes and at high photon energies pair production is the prevailing initial energy transfer mechanism.

The mass absorption coefficients for these various processes in water have been plotted against incident photon energies in diagram I. The mass absorption coefficient is defined as $\frac{f\mu}{\rho}$. where ρ is the density in grams cm^{-3}, and f is a correction factor for scattering, fluorescence losses and bremsstrahlung emission. The true mass absorption coefficient is essentially the sum of all the individual coefficients for the effects discussed above: (see legend on diagram)

$$\frac{f\mu}{\rho} = \frac{\tau}{\rho} + \frac{\sigma_a}{\rho} + \frac{\sigma_s}{\rho} + \frac{k}{\rho}$$

energy contributions from scattered photons are often neglected to a first approximation. At very high incident photon energies photonuclear reactions may occur of the general form (γ,n) or $(\gamma,p)_j$ there is a high
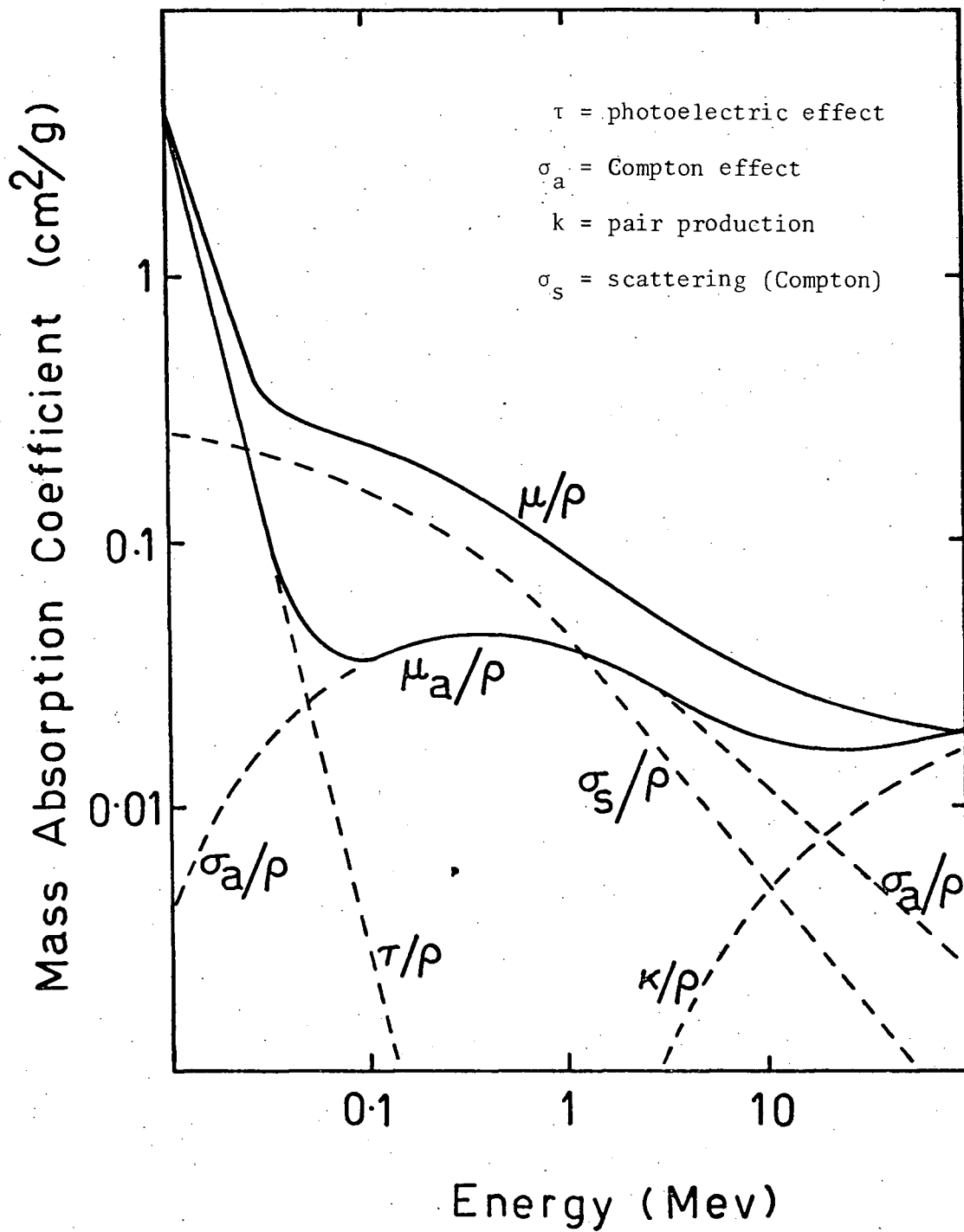
Diagram 1. Mass absorption coefficients for the various processes in water.

threshold for these reactions and one can justifiably assume that in most cases they offer no significant contribution to the total energy absorbed.

Particle radiations

As a high energy charged particle travels through a medium energy may be transferred via direct collisions and excitations with the predominant appearance of ionised and excited atoms and the production of radiation. At lower energies the particles will be involved in elastic scattering and inelastic collisions to a more significant degree.

The interactions of heavy particles such as alpha particles and those of electrons of the same energy in any absorbing medium can be only qualitatively compared because the electrons will have a greater velocity and as such cause less specific ionisation. With a beam of high energy electrons as an incident radiation source the energy transfer processes that must be considered are:

      (i)   elastic scattering, deflection

    (ii)   inelastic scattering and excitation

   (iii)   emission of bremsstrahlung radiation.

There will be a statistical variance in the number of collisions between the incident particle and the electrons of the medium and consequently in the energy transferred during these events. This is indicated by the ranges of the particles in a given absorber, and in the case of an electron (which can lose a substantial amount of its energy in one collision) the spread is even more pronounced.

(i)   elastic scattering arises from the deflection of the incident electron without loss of energy by the coulombic fields about the nuclei of the medium; the process is most important for low energy electrons and materials of high electron density. Any large angle deflections will be from nuclear scattering.

(ii)   inelastic scattering occurs when the incident electron interacts with these coulombic fields of the medium and a large fraction of the energy of the incident electron may be transferred in a single collision. Energy imparted to the electron of the medium experiencing a collision is often sufficient to cause this electron to take part in secondary collisions itself. These primary and secondary events both lead to ionisation and excitation of the atoms in the absorbing material and are the dominant process for the energy loss of medium energy electrons <1 MeV below which bremsstrahlung emission is not an important factor.

(iii) Bremsstrahlung radiation is emitted to conserve energy and momentum relationships when a high speed electron is deaccelerated in the environment of a nucleus of the atoms in the absorbing material and is predominant mode of energy loss for electrons >10 MeV. The rate of loss of energy $\frac{-dE}{dx}$ is proportional to $\frac{z^2 Z^2}{m^2}$ where z, Z are the charges on the particle and nucleus respectively, and m is the mass of the particle.

The range of the electron

The track of a charged particle passing through a medium will not necessarily be a straight one, and for electrons in particular the

true range is much greater than that determined experimentally, owing

to the appreciable and diversified scattering already discussed. However

the average range is still dependent on the rate of loss of energy of

the incident electron -- referred to as the stopping power of the material

with respect to that particle. In Bethe's formula below this loss

per unit length is related to both the characteristics of the medium

and the incident particle.

$$-\left(\frac{dE}{dx}\right)_{collective} = \frac{2\pi e^4}{m_o v^2}.N.Z\left[\ln\frac{m_o v^2 E}{2I^2(1-\beta^2)} - (2\sqrt{1-\beta^2} - 1 + \beta^2)\ln 2 + 1 - \beta^2 + \frac{1}{8}(1 - \sqrt{1 - \beta^2})^2\right] \text{ ergs cm}^{-1}$$

v = velocity of incident particle, cm sec^{-1}.

$\beta = \frac{v}{c}$, c is the velocity of light, cm sec^{-1}.

I = mean excitation potential of the atoms, ergs.

N = number of atoms per c.c. of stopping material.

e = charge on electron, esu.

m_o = rest mass of the electron, grams.

Z = atomic number of the stopping material.

The stopping power is $-\left(\frac{dE}{dx}\right)_{collective}$, which divided by the

density of the material ρ gives the mass stopping power. The lower the

incident energy of the particle the more readily will it reach thermal

energies. In diagram 2 the number of incident monoenergetic electrons

that penetrate to a certain position in the absorbing material has been

plotted as a function of distance. The tail of the curve represents

the distribution of ranges and the mean range R_m is shown with the

extrapolated range R_{ex}, the latter value being the one used in experi-

mental work. (It is only possible to determine a maximum range for
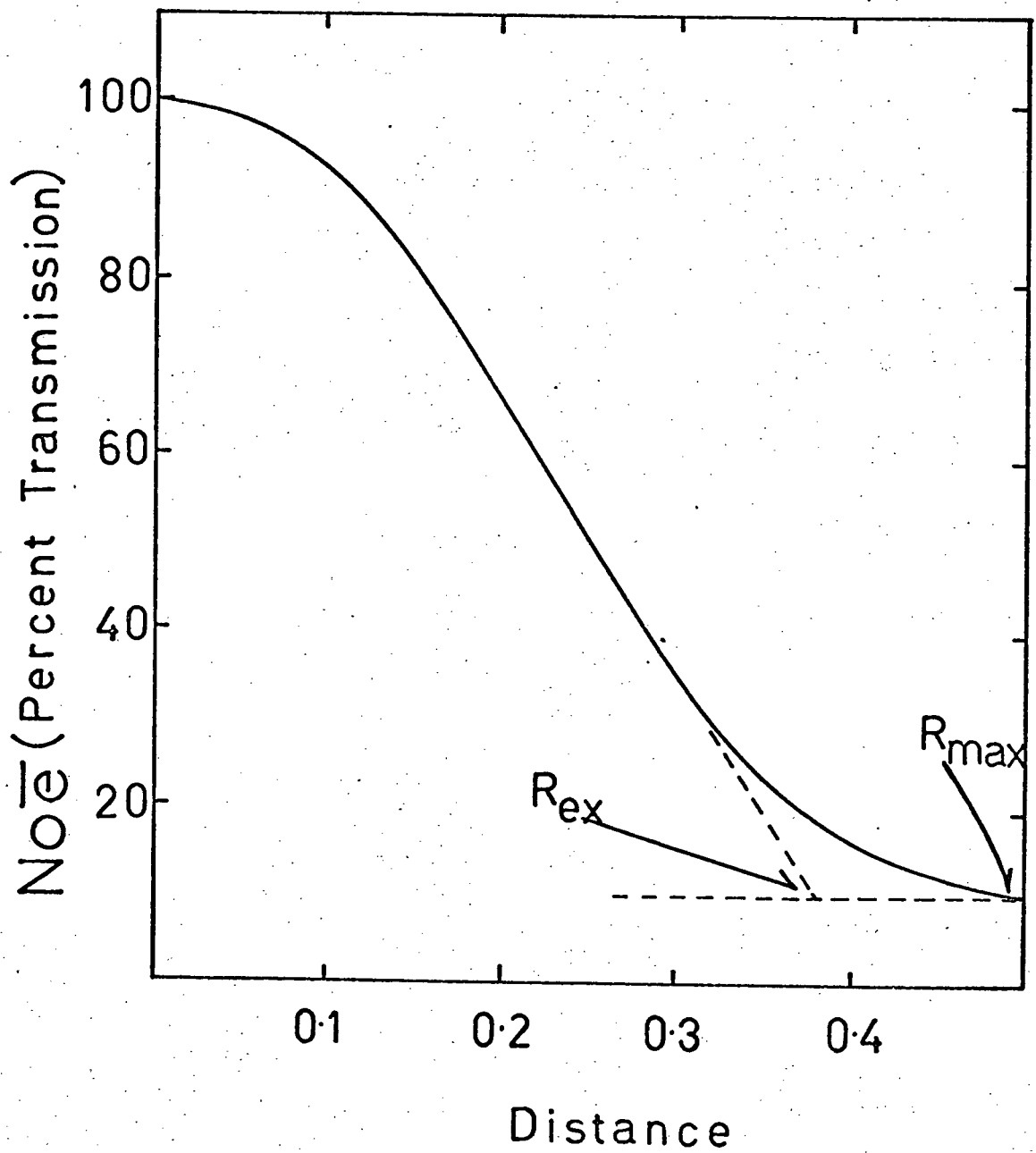
Diagram 2.   Range of a beam of monoenergetic electrons
in an absorber

non-monoenergetic beams by means of a penetration study.)

As the electron spends a time inversely proportional to its velocity within an interaction distance of the atomic electrons any changes in its momentum and energy transfer must be accomplished within this period. However in relativistic regions the kinetic energy of the particle exceeds its rest-mass energy ($\beta \rightarrow 1$) and significant variations in the $\ln(1-\beta^2)$ term lead to an increase in the specific ionisation $(-dE/dx)_{collective}$ paralleling the increase in v; the interpretation of this is based on the apparent shorter time of collision (thereby increasing the impact parameters) due to the Lorentz contraction. At non-relativistic velocities, $(\frac{-dE}{dx})_{collective}$ decreases as v increases.

Cerenkov radiation

The instantaneous (within 10^{-13} seconds) emission of light at wavelengths in the I.R., visible and U.V. during the irradiation of various media with fast charged particles is classified as Cerenkov radiation and has special significance in any study of the absorption and emission effects in irradiated liquids. The intensity and duration of the luminescence is such that it can mask weak or very short lived emission or absorption and therefore appropriate experimental precautions must be taken. The duration of the emission is determined by the velocity of the charged particle and the length of its track before it slows down to below-threshold conditions. The emission arises from relativitic considerations. If the velocity v of a fast charged particle moving in a medium of refractive index n exceeds the phase velocity of light $(\frac{c}{n})$ in the same medium, then an electromagnetic shock wave is produced at an angle to the track of the particle as a result of the

polarisation and subsequent relaxation of the molecules in the immediate

vicinity of the track.

The threshold condition is therefore

$$n\beta >> 1$$

where β is the relativistic velocity $\frac{v}{c}$. The angle θ at which the light

is emitted is related to the track direction

$$\text{Cos } \theta = \frac{1}{n\beta}$$

and for water if n = 1.332, β will be 0.751 corresponding to 265 KeV

electrons for the threshold particle energy.

Dose and yield

The yield of a species formed or destroyed in the chemical

processes induced by radiation is expressed in terms of the number of

molecules per unit of absorbed energy.

$$G_{(x)} = \frac{\text{number of molecules of x formed}}{100 \text{ eV absorbed energy}}$$

Evaluation of the absorbed energy is therefore critical and a range of

techniques are available to measure this energy. In dosimetry the

common unit of absorbed dose is the rad. One rad is equivalent to

the deposition of 100 ergs or 6.24×10^{13} eV per gram of material.

Irradiation of liquid water

The radiation chemistry of liquid water is a remarkably

complex subject whose theoretical tenets based on physical and chemical

evidence are not fully understood even at the present moment. To

emphasise the changing environment in the vicinity of the incident

charged particle as it travels through the liquid medium this section

will be presented in three chronological stages following the impact of the primary particle.

(i) (a) physical 10^{-18} to 10^{-16} seconds

    (b) energy transfer effects

(ii) physicochemical 10^{-13} to 10^{-7} seconds

(iii) chemical $>10^{-7}$ seconds

In view of the exponential increase in the number of papers on the radiation effects in biologically important molecules and in vitro systems where water plays a major role, it would be justified to complete the sequence with

(iv) biochemical, biological $>10^{7}$ seconds, even if discussion as such is beyond the scope of this thesis. The sequence is illustrated in diagram 3.

(i) a. <u>Stage I - physical</u>

The absorption of radiation is a very fast process and does not produce a simultaneous response that can be experimentally observed other than Cerenkov radiation. The primary electron (or Compton electron in the case of incident X or γ rays) follows a linear track at high energies but is deflected as it slows down; secondary ionisations and excitations are produced along this track giving rise to both low ($\leqslant 10^{2}$ eV) and high ($>10^{2}$ eV) secondary electrons. The latter, if sufficiently energetic will branch off to form another shorter track referred to as a δ ray, along which the remaining energy will be deposited. The low energy secondary electrons suffer further deflections causing ionisation and excitation in a defined area of the medium.

The energy of the primary particle is thus deposited along these

Impact of Primary Particle

0 secs		Physical Stage
10^{-18} secs		$\bar{e}$ high energy
10^{-16} secs		
		$\bar{e}$ sub excited
		Physicochemical Stage
10^{-13} secs		$\bar{e}$ thermal
10^{-11} secs		$\bar{e}$ solvated
10^{-8} secs		$\bar{e}_s$ reacts in
10^{-7} secs		chemical stage
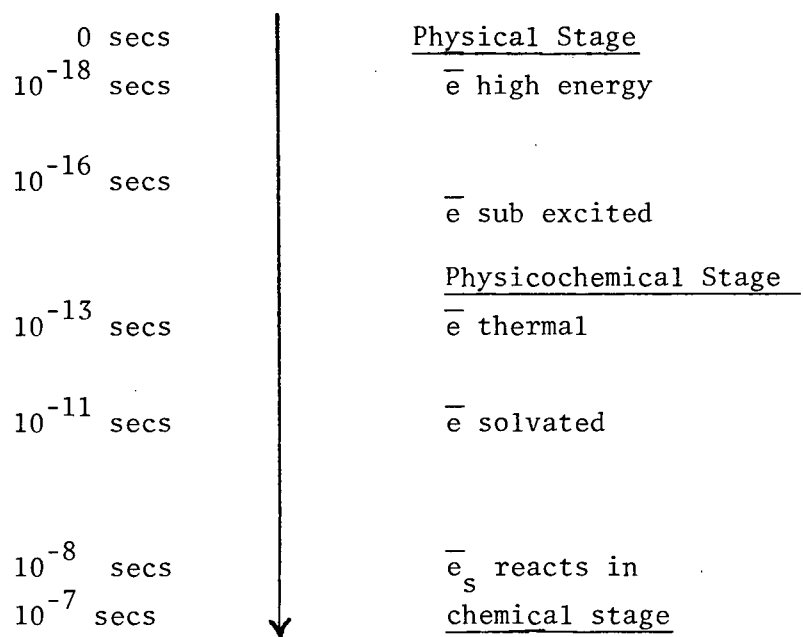
Diagram 3: Sequence of events after the impact of the incident particle (41)

tracks as a number of events or spurs; about 60% of the total energy is transferred to the medium in this way. A spur is considered to be an average deposition of 100 eV and will be a cluster of electronically excited species, positive ions and electrons, all of which now enter the physicochemical stage.

(i) b. Energy transfer effects

The distance between the spurs is related to the nature of the primary particle and is calculable from a knowledge of the rate of energy transfer to the medium. The linear energy transfer or L.E.T. formally expresses this as a rate of energy loss of the incident particle in eV per $\overset{\circ}{A}$, and puts the energy loss for different particles on a quantitative basis. The L.E.T. increases along the track as the particle slows down implying that the spurs become closer together towards the end of a track-- and with high L.E.T. tracks the spurs will necessarily overlap. Since the chemical products of radiolysis are governed by the behaviour of the species formed in the spur, and the spatial distribution of the spurs by the L.E.T. characteristics of the particle, L.E.T. effects are extremely important.

For a typical Co^{60} γ-ray the L.E.T. is 0.02 eV per $\overset{\circ}{A}$ which is small and the spurs will be relatively isolated. Low energy electrons have L.E.T. values increased by an order of magnitude while a heavy alpha particle has a high L.E.T. of $\sim$ 10 eV per $\overset{\circ}{A}$.

The model of spurs, tracks and γ-rays has been elaborated (6,7) in an attempt to give a more realistic picture of the arbitrarily classified secondary electrons in the light of these different L.E.T. effects.

An energetic secondary electron or δ-electron of energy greater than 5000 eV will form its own branch track and because of the low L.E.T. the spurs will be well separated, of the order 10^3 Å apart. As the δ-electron loses energy the L.E.T. increases and at energies below 5000 eV the spurs begin to overlap giving rise to a short track. Finally as the δ-electron approaches energies of 500 to 100 eV it becomes difficult for the electron or products of its ionisation power to move far from their origin, thus giving rise to a densely packed area of ionisation and excitation with a visualised pear-shape geometry, often referred to as a blob. The secondary electrons with energies below 100 eV will form clusters of ionisations in isolated spurs.

As the molecular products, formed in intraspur reactions or on the recombination of ion pairs within the spur, differ in yield from those attributed to say radical reactions between species diffusing out of the spurs, it is not suprising that variations in the intensity and origin of the ionising radiation lead to different yields.

(ii) Stage II - physicochemical

The cluster of ionised and excited species designated as a spur may lose energy by collision and dissociation into radicals. Solvent quenching of excited species can occur within 10^{-12} seconds and metastable states are thought to return to the ground state by non-radiative processes. As about 30 eV is expended on average per ion-pair produced, a typical spur will contain three ion-pairs or six radicals. Energetic electrons have already been discussed but a sub-excited electron ($<$ 10 eV) can become thermalised and within 10^{-11} seconds (the dielectric relaxation

time of water) solvated.

The position of the thermalised electron with respect to the positive parent ion must be carefully considered -- if the thermal energy of the electron exceeds the attractive potential energy resulting from the coulombic field of the concomittant positive ion, the electron will not be recaptured. The net separation of the ion pair due to random walk is critical and for aqueous solutions two opposing theories relating to the yields of molecular products are based on different evaluations of this parameter. Obviously media of high dielectric constants will permit the electron to travel further before thermalisation.

The Samuel-Magee model (8) assumes that recapture does occur in the coulombic field, while the Lea-Platzman model permits the electron to escape before thermalisation. Current spectroscopic (10) and chemical evidence (11) tend to favour the latter model while modifications to the former accounts for some discrepancies, but there is still a large difference in the estimates of the mean free path of the escaping electron.

The diffusion of radicals begins in this stage and the spur is therefore increasing in size which rather invalidates the accepted first approximation of regarding the spur as having spherical geometry. Unfortunately it is also during this period that one requires good values for spur size and overlap in mechanistic calculations. If the species escapes from the spur it must eventually react with another radical, solute or solvent molecules, perhaps at diffusion controlled rates. A theoretical treatment of such a one-radical one solute problem has been given by Kupperman (12) and extended to more complex systems.

The mechanisms occuring during the physiochemical stage are

$$H_2O \longrightarrow H_2O^+ . \bar{e} \text{ , possibly } H_2O*$$

$$H_2O^+ + H_2O \longrightarrow H_3O^+ + OH$$

$$H_2O* \longrightarrow H + OH$$

$$\bar{e} \text{ thermal} \longrightarrow \bar{e} \text{ aquated}$$
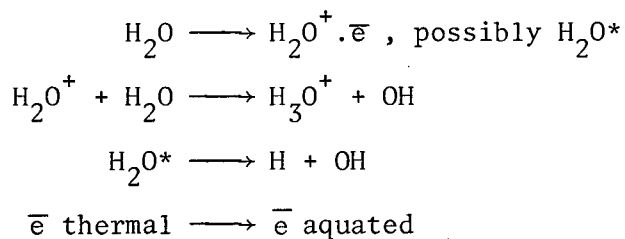
(iii) **Stage III - chemical**

Fluorescence from electronically excited states may be observed and, as low energy electrons in the δ-ray area will give rise to disallowed excitations, phosphorescence on a delayed time scale. Unimolecular reactions involving a breakdown of the original molecule, rearrangements (H atom migration) bimolecular ion-molecule reactions, dissociative and non-dissociative charge transfer (depending on the stability of the ions formed) are all postulated to account for the radiolytic products.

The irradiation of liquid water at pH 7 with a beam of high energy electrons gives rise to the following products; the G values are in brackets.

$$H_2O \longrightarrow H_2(0.42), H_2O_2(0.71), H(0.6), OH (2.2)$$

$$\bar{e} \text{ aq}(2.3) \text{ and } (H.OH, H_2O*)?$$
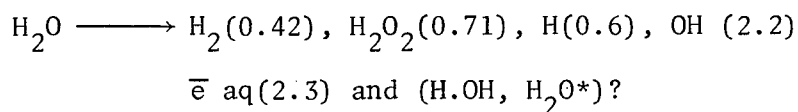
The following intra spur mechanisms in the previous stage lead to the product formation observed:

$$\bar{e} \text{ aq} + \bar{e} \text{ aq} \longrightarrow H_2 + 2OH^- \text{ aq}$$

$$H + H \longrightarrow H_2$$

$$OH + OH \longrightarrow H_2O_2$$

$$H + OH \longrightarrow H_2O$$

$$H + \bar{e} \text{ aq} \longrightarrow H_2 + OH^-$$
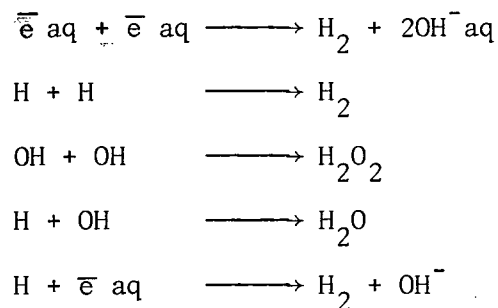
If the species diffuse from the spur they can also react with solvent or solute molecules S

$$H, \overline{e} \text{ aq, OH } + S \longrightarrow \text{ products.}$$

These are the main reactions in the irradiation of liquid water although some others relevant to the behaviour of excited water, itself a controversial species (13,14), have not been included.

The hydrated electron

(i) In 1962 the publication of a paper describing an electron pulse-induced broad absorption in the visible region of the spectrum which was positively attributed to the hydrated electron, climaxed several years of experiments and predictions in different laboratories and opened up an entirely new concept of primary reaction mechanisms. (In retrospect the now classic paper of Hart and Boag (15,16) not only characterised this curious species but also with the technique of pulse radiolysis and solute scavenging provided the first real basis for the determination of absolute rate constants).

Perhaps the success of the free radical hypothesis of Weiss (17) in accounting for the irradiation processes in liquid water was in part the reason for the prolonged lack of interest in the secondary electrons. However, in 1953 Platzman (18) in a theoretical paper had questioned the reaction

$$\overline{e}_{thermal} + H_2O \longrightarrow H + OH^-$$
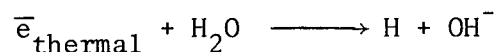
on the grounds that there was a significant time delay between the reaction time and the time required to utilise the hydration energy which made the reaction energetically feasible. He continued "...for this reason the electron becomes hydrated....I mean (here) that the electron polarises the dielectric and is bound in a stable quantum state to it.....there is time for the hydration to take place, which must as

Dr. Onsager said be a minimum of the relaxation time 10^{-11} seconds."
The implications of Platzman's remarks were not fully realised for many
years although Stein (19) in 1952 had suggested that the hydrated electron
might be present in an irradiated methylene blue system.

By the late fifties sufficient work had been reported to establish
the fact that there had to be two different reducing species in
irradiated waters: there was no other way of interpreting the anomalous
kinetics in the variety of aqueous systems investigated. These included
the formic acid and ferrous-cupric (Hart (20)) the chloroacetic acid (Hayon
& Weiss (21)) the peroxide (Barr & Allen (22)) and the methanol-
cupric sulphate systems (Baxendale & Hughes (23)). When the dominant
reducing species in irradiated neutral solutions was shown to have unit
negative charge (Czapski & Schwarz (24) later confirmed by Collinson
et al (25) and Dainton & Watts (26)) the role of the electron in these
systems was no longer speculative.

The transient absorption reported by Keene (27) in his pulse
radiolysis experiments in aqueous solution had been tentatively attributed
to a hydrated electron (Matheson (28)) in view of the fact that the
absorption did not appear in solutions containing electron scavenging
solutes.

The hydrated electron identified by Hart & Boag in their
sensitive combination of flash spectroscopy and pulse radiolysis is now
known to be a chemical entity in its own right with diffusion and inter-
action properties. In the six years since its discovery the rate constants
for some six hundred of its reactions with inorganic, organic and bio-
chemical systems have been compiled (29); most of these are diffusion

controlled rates and are among the fastest reactions known. Parallel
to the investigations of electron-solute interactions were experiments
designed to produce the hydrated electron in different ways for it had
been immediately recognised that many reactions previously attributed
to the hydrogen atom, at a suitable pH may have been intitated by the
hydrated electron, its conjugate base.

At the present time it is generally accepted that $\bar{e}$ aq is the
precursor to hydrogen whenever water is reduced; as a most powerful
reducing specie, $\bar{e}$ aq may be generated radiolytically, photochemically,
electrolytically, by chemical reduction, from H atoms, by photo-induced
electron emission from metals and from stable solvated electrons in
other media (5). The deuterated electron has also been prepared and
its reactions studied (30).

(ii) A physical model

The precise sequence of events that lead to the formation of
a solvent sheaf about the electron and the nature of the stable quantum
state in which the electron is then trapped, continues to invoke much
discussion as the experimental evidence is not unambiguous.

Two different theories on the immediate fate of the thermalised
electrons will be briefly discussed. As an electron approaches thermal
energies it is still moving through the water relatively quickly and
although it affects polarisation of the water molecules near the track
it is not long enough in the region to be trapped by this polarisation;
if there already exists a region of accidental polarisation due to the
random thermal motions of the molecules themselves then the water dipoles
will be polarised to a more significant degree in the field of the excess

electron. In liquid water both electronic and orientational polarisation
are important, the finite time associated with the latter due to molecular
rotation. The dielectric relaxation time of water is 10^{-11} seconds.
Schiller (31) regards the dielectric relaxation time in the trapping
procedure as the decisive paramter. He assumes the track and spur model
and considers the time-dependent dielectric properties of the medium
with a non-conservative electric field; the probability of trapping the
electron increases as the relaxation time (τ) increases. Investigations
on electron capture in media of different τ but similar static and optical
dielectric constants (liquid water, supercooled water and ice; variation
of 10^6 in τ) have supported his ideas (32).

The other model of electron capture is based on a time-independent
dielectric constant and a static electric field. Here Freeman and Fayadh
(33) use the cavities present in the liquid structure as the initial
trapping centres, and suggest that the limiting factor in the mobility
of the electron is the physical migration of these cavities. Experimental
evidence is given.

At the conclusion, on either model, the electron is trapped
in a potential well with partial orientation of a second and third layer
of water molecules in the outer solvation sheaf, although thermal agitation
will cause these arrangements to be time-dependent. The number of water
molecules in the inner solvent sheaf could be from four to six, it is
not known, and there may be a range of binding energies for the electron
in its trap, or traps of different depth. To what extent this general
picture can be responsible for the broad absorption spectrum of the hydrated
electron, and electrons solvated in other media, is open to speculation.

The absorption spectrum of the hydrated electron (see diagram 4) is evident at 5000Å with a maximum at 7200Å and shows no convergence limit at 5400Å. Trapped electrons in ice have the same λ_{max} and featureless absorption spectrum although they are in an ordered matrix but it is interesting to note an increase in intensity in the near ultraviolet region has been reported (34). Yet in another study (35) the appearance of a distinct shoulder in the lower wavelength region ∿5500Å to 6000Å was observed for the absorption spectra of some frozen aqueous solutions and crystalline ice. A narrowing of the absorption band was also seen down to 200°K by these workers; such behaviour has not been observed by others. It may well be that the mode of introduction of the electron into a solution or a frozen matrix may account in part for these discrepancies. The assymmetry of the spectrum of the high energy side of the spectrum of $\bar{e}$ aq has also been observed for ammoniated electrons, but neither spectra shows any discernible fine structure.

Dorfman has found a correlation between the static dielectric constants and the values of λ_{max} for electrons solvated in a series of alcohols (36).

The extinction coefficient for $\bar{e}$ aq in the region of λ_{max} is $\approx 10^4$ litre mole^{-1} cm^{-1} and thus the transition corresponding to the energy of λ_{max} must be allowed. Jortner (37) published variational calculations based on a quantum mechanical model which attributes the λ_{max} to a $(2p \leftarrow 1s)$ transition in the potential well. He treated the solvent as a continuous dielectric medium in which an excess electron has been caught in a self-induced polarisation trap. The electron is incompletely confined to a cavity of uniform field and experiences a decrease in the

G$_{e_{aq}^-}$ X   EXTINCTION COEFFICIENT

(X 10^{-4})

WAVELENGTH Å
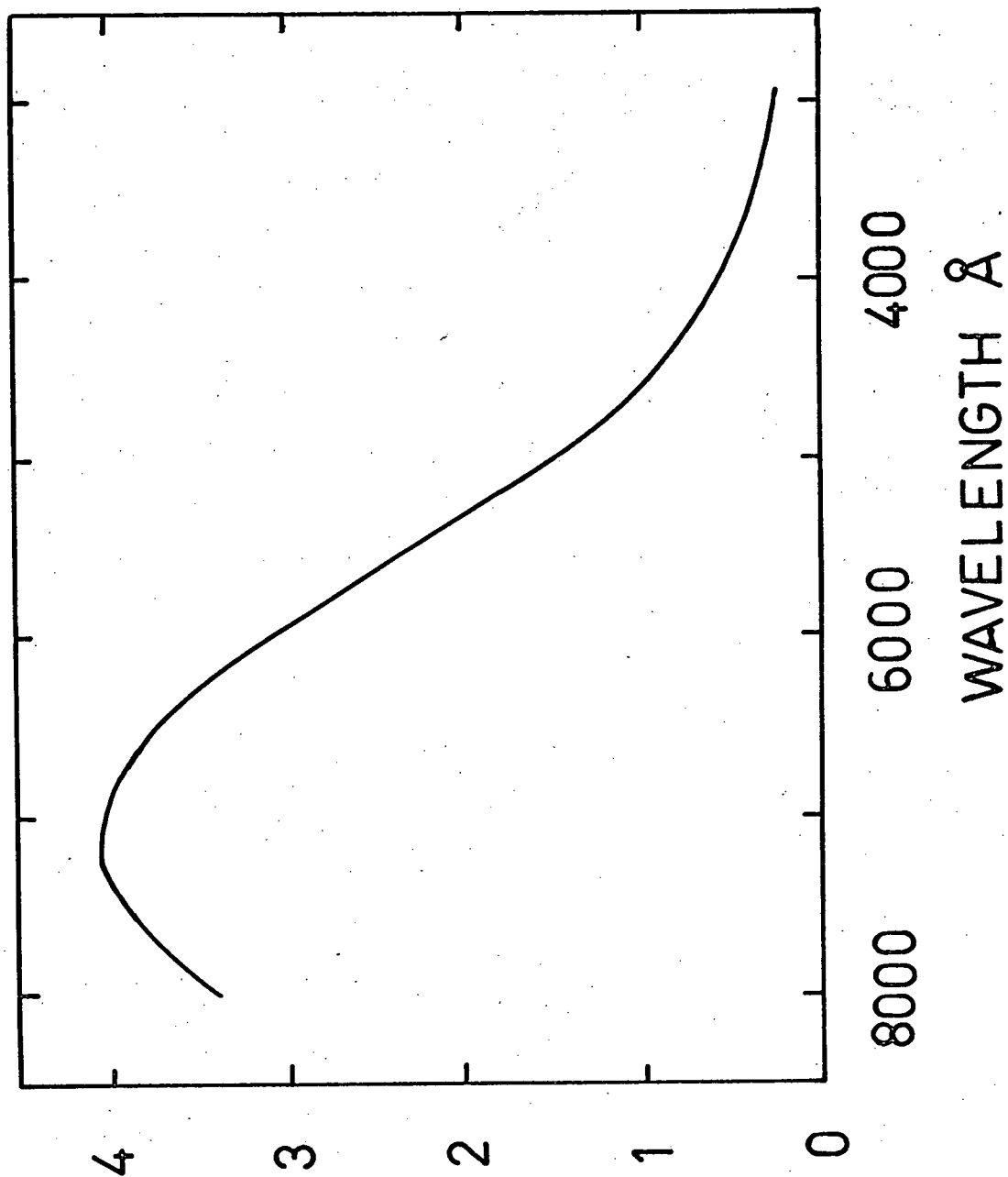
Diagram 4.   The Absorption Spectrum of e̅ aq

coulombic field as it wanders outside the inner solvent sheaf into the bulk medium. The parameters that define the trap are the static and optical dielectric constants.

With hydrogenic wave functions he anticipates the first excited state to be a 2p state, and the (2p ← 1s) transition to occur at an energy $E(h\nu) = 1.35$ eV, the oscillator strength being $fi = 1.1$. The cavity radius under these conditions equates to zero. Experimentally λmax equates to 1.75 eV, $fi = 0.8$ and the radius of influence of the hydrated electron to be 2.5 to 3.0Å. The most recent determination is 2.9Å (38). On this hydrogen=type model treatment the first transition may correspond to three quarters of the well depth (diagram 5(a)). Higher transitions (3p ← 1s) will be very weak if they occur at all as for a one electron system the sum of the oscillator strengths has to be unity; the broad absorption band certainly shows no fine structure but it may be masking a very weak band.

Jortner's model encounters more complications in explaining the nature of the hydrated electron than the ammoniated electron (37). The temperature dependence of max for $\overline{e}$ aq was predicted to be -3.3 $\times 10^{-3} \lesssim \dfrac{dE}{dT}$ max $\leq -2.2 \times 10^{-3}$ (eV per degree) and recent results (38) report a shift of $-2.9 \cdot 10^{-3}$ eV per degree in Co^{60} γ radiolysed aqueous systems. The initial optical density of λmax at 10°C had decreased by 70% at 96°C. It appeared that the radius of the hydrated electron was increasing. However pulse radiolysed systems indicated no such behaviour in λmax over the same temperature range. Chemical evidence of photo bleaching and photoconductivity (39) ambiguously relate to the proposed

2p upper bound state of solvated electrons and the appearance of

temperature dependent λ max for other solvated electrons outside the

framework set by $\bar{e}$ aq and $\bar{e}$ ammn. strongly suggests the need for a

modified or alternative model. It is not intended to discuss these models

in detail but to emphasise the importance of the excited state in the

alternative theories in accounting for the transitions associated with

the observed λ max. The broadness, asymmetry and lack of fine structure

must also be accounted for. The energy of λ max has been likened to an

ionisation potential (I_p), to release of the electron from its trap. The

hydration energy of the $\bar{e}$ aq was calculated to be 1.72 eV (40). The

relationship between any polarisation energy of the solvent, I_p and the

hydration energy ΔH is shown in diagram (5b). Variation in the size

of traps, and thermal motions of the solvent sheaf itself may give

rise to the broadness of the spectrum (5d). Even if the traps had

essentially the same immediate environment in the ground state there

could still be a wide variation in this environment at excited levels.

The latter may in fact be a continuum analogous to the conduction band

of a semi conductor into which the electrons are excited by wavelengths

less than λ max (5c). The possibility of a symmetrical charge transfer

absorption in combination with an ionisation continuum has also been

proposed in a discussion of these models in (41).

If the hydrated electron were excited i.e. photolysed at

suitable energies, into this unspecified upper state and its behaviour

followed through suitable means one could distinguish between the models

through the changing co-ordinates of λ max; an attempt to excite the

electron from this state into an even higher one would also give valuable

$$E_\lambda = E_\lambda \max$$
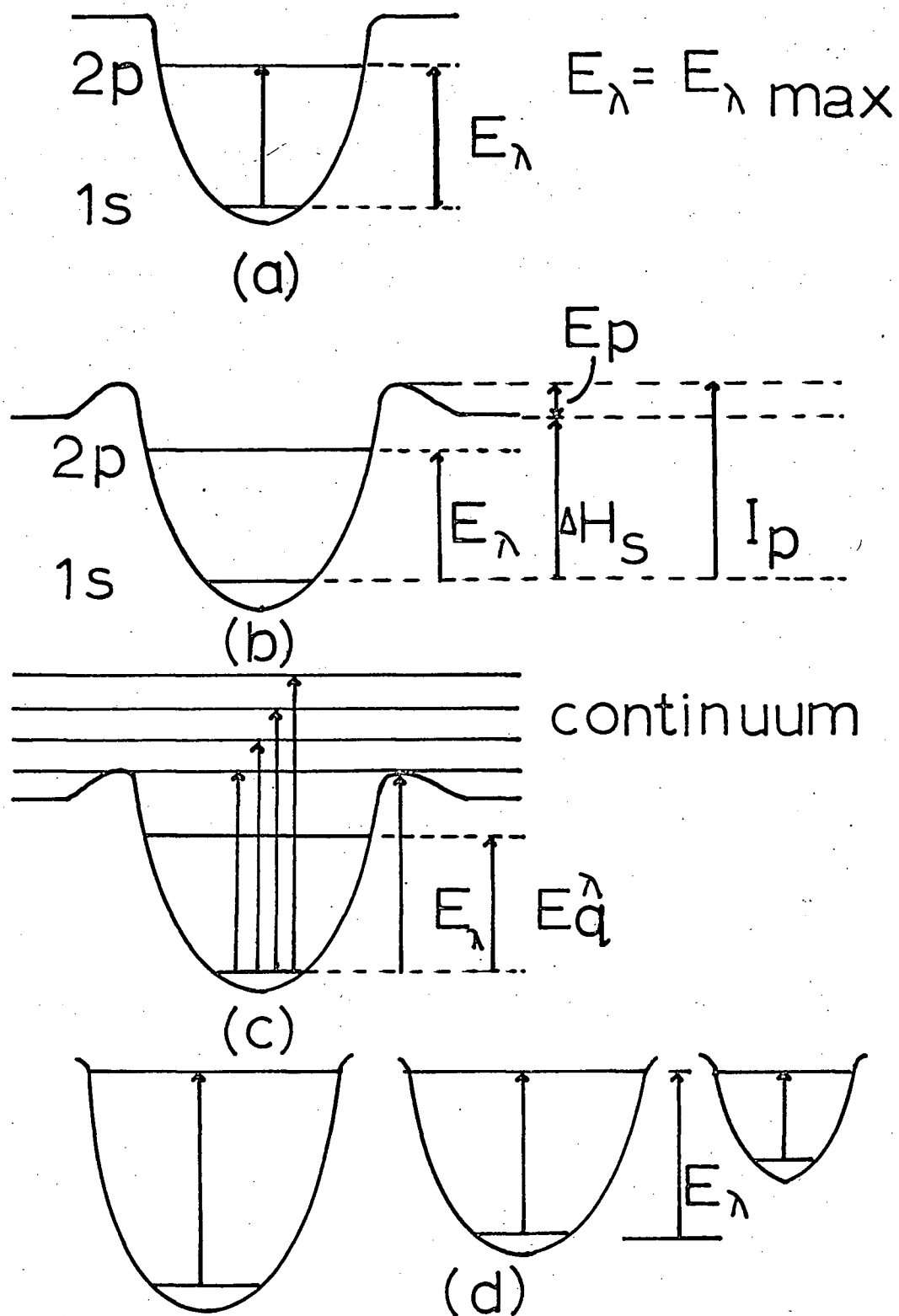
Diagram 5. Model relating $E_{\lambda MAX}$ to the

Structure of the Hydrated Electron

information.

The work described in this thesis proved to be a necessary preliminary basis for experiments designed to study the nature of the excited state of the hydrated electron, the formation and decay of which may be followed spectroscopically at wavelengths approaching λmax.

(iii) <u>Fate of the hydrated electron</u>

The processes that contribute to the loss of the hydrated electron vary in efficiency with the dose rate of the ionising radiation, the pH of the medium, other species that may be present as impurities or scavengers and the temperature of the solutions.

$$H_2O \longrightarrow \bar{e}\ aq,\ H,\ OH,\ H_2,\ H_2O_2,\ H_3O^+,\ OH^-$$
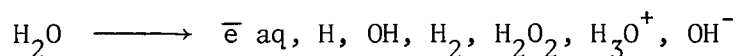
The following reactions may occur during and after the irradiation; only OH^- and H_2 do not react with $\bar{e}$ aq.

	pH	Rate (29) $M^{-1}\ sec^{-1}$
(1) $\bar{e}\ aq + \bar{e}\ aq \longrightarrow H_2 + 2OH^-aq$	10.5	$4.5 \cdot 10^9$
(2) $\bar{e}\ aq + OH \longrightarrow OH^-\ aq$	10.5	$3.0 \cdot 10^{10}$
(3) $\bar{e}\ aq + H \longrightarrow H^-\ aq$	10.5	$2.5 \cdot 10^{10}$
(4) $\bar{e}\ aq + H_3O^+ \longrightarrow H + H_2O$	4.5	$2.32 \cdot 10^{10}$
(5) $\bar{e}\ aq + H_2O \longrightarrow H + OH^-\ aq$	8.4	$1.6 \cdot 10^1$
(6) $\bar{e}\ aq + H_2O_2 \longrightarrow \cdot OH + OH^-\ aq$	7	$1.23 \cdot 10^{10}$

With nanomolar concentrations of $\bar{e}$ aq from low dose rates (50 rads per pulse) the decay is a first order process; as the dose increases the $[\bar{e}\ aq]$ moves to the micromolar region and the decay now resembles second order kinetics. At higher doses the hydroxyl radicals, hydroxonium ions and hydrated electrons are all in sufficient concentration to give classical second order kinetics and the rates are diffusion controlled. When $[\bar{e}\ aq]$ is in millimolar concentrations the technical

situation becomes more complex as the halflife is considerably reduced and the interpretation of the kinetics in a classical sense appears ambiguous. The dominant decay mechanism is

(1) $\bar{e}$ aq + $\bar{e}$ aq $\longrightarrow$ H$_2$ + 2OH$^-$ aq $\quad\quad$ k$_1$
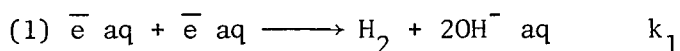
but radical-radical and radical-ion reactions account for nearly half of the total number of processes that must be considered before a rate constant for the primary decay can be evaluated. Fortunately not all of these reactions are kinetically significant under any given set of experimental conditions and with the judicious use of pH and scavenging solutes many of the reactions can be at least controlled if not eliminated. The radical reactions are listed in Table I below

Table I

Reaction	pH	k $M^{-1}sec^{-1}$
H + H $\longrightarrow$ H$_2$	2.0	$1.0 \cdot 10^{10}$
H + OH $\longrightarrow$ H$_2$O	3.0	$1.2 \cdot 10^{10}$
OH + OH $\longrightarrow$ H$_2$O$_2$	7.0	$4 \cdot 10^9$
H + H$_2$O$_2$ $\longrightarrow$ H$_2$O + OH	2.1	$9 \cdot 10^7$
H$_3$O$^+$ + OH$^-$ $\longrightarrow$ 2H$_2$O	7.0	$1.43 \cdot 10^{11}$

Under high dose rate conditions the species in neutral water that could appreciably interfere with the "pure" biomolecular decay are the hydroxyl radical and the hydrogen atom. In the presence of a calculated amount of methanol (or higher alcohol) the hydroxy radicals will be removed with the hydrogen atoms; in both instances the relatively inert CH$_2$OH radical is produced.

(7) $\quad$ H + CH$_3$OH $\longrightarrow$ CH$_2$OH + H$_2$ $\quad\quad$ K$_7$ = $1.7 \cdot 10^6$ M^{-1}sec^{-1}

(8) $\quad$ OH + CH$_3$OH $\longrightarrow$ CH$_2$OH + H$_2$O $\quad\quad$ K$_8$ = $5.1 \cdot 10^8$ M^{-1}sec^{-1}
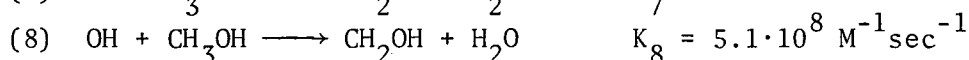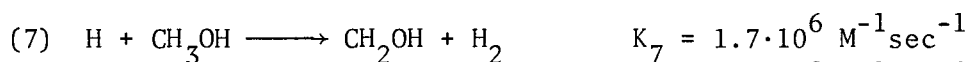
In addition common impurities such as dissolved O$_2$ or CO$_2$ in

the liquid will have appreciable effects on the initial rate of decay

of the hydrated electron and must be removed as much as possible.

(9) $OH + CO_3^= \longrightarrow CO_3^-$ pH 11, $K_9 = 3.0 \cdot 10^8 \ M^{-1}sec^{-1}$

(10) $\bar{e} \ aq + O_2 \longrightarrow O_2^-$ pH 7, $K_{10} = 2.10^{10} \ M^{-1}sec^{-1}$

The reaction with $CO_3^=$ is particularly undesirable as the CO_3^-

ion absorbs at 6000Å. Peroxides and other radiolytic products are

dealt with according to the prevailing experimental conditions. In

many instances however the effective concentration of competing species

does not decrease as rapidly as the concentration of $\bar{e} \ aq$ (30).

The Problem

The predominant decay mechanism of the hydrated electron in

neutral water under high dose rate conditions is

(1) $\bar{e} \ aq + \bar{e} \ aq \ \underset{\longleftarrow}{\longrightarrow} \ (e)_2^{2-} \ aq \longrightarrow H_2 + 2OH^- \ aq$
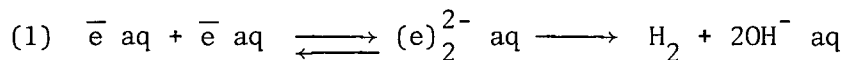
and would be described in a classical sense as a bimolecular decay.

(The transient $(e)_2^{2-} \ solv$ species has been identified in several other

systems, liquid, glassy and solid matrices (34,42,43,44) generally

through the absorption or e.s.r. spectra.) The rate constant for this

reaction is diffusion controlled but the literature contains an abundance

of data that fits neither a first order nor a second order kinetic

treatment. There would appear to be a transition from one mode of decay

to another within a very short time and thus the data not unexpectedly

shows variations according to the radiation source, the duration and

intensity of pulsed radiation and the speed with which the decay can

then be followed. The different values for K_1 were all within an order

of magnitude (see Table II below) until the startlingly high value of

$3.2 \ 10^{11} \ M^{-1} \ sec^{-1}$ was reported by Klein and Warner (45) in 1966; this is the fastest reaction in the liquid phase ever published, and they suggest that the model used to explain the radiation chemistry of water at low dose rates is inadequate at very high dose rates such as they had employed. Other values for k_1 and recently calculated are given below.

Table II

Reference	Author	K $M^{-1} sec^{-1}$	Technique	Dose Rate	pH
45	Klein.Warner	$3.2.10^{11}$	p.r.	$\sim 10^{25} eV/\ell^{-1} sec^{-1}$	>8
38	Gottschall.Hart	6.3 ± 1.10^9	$Co^{60}\gamma$	$\sim 10^{19} eV/\ell^{-1} sec^{-1}$	>8
46	Matheson.Rabani	$5.5 \pm 0.75.10^9$	p.r.	high	7-14
47	Dorfman.Taub	$<7.0.10^9$	p.r.	high	12
30	Hart.Fielden for($\bar{e}d+\bar{e}d$)	$6.0.10^9$	p.r.	$\sim 10^{24} eV/\ell^{-1} sec^{-1}$	pD13.4

In order to examine the $\bar{e} \ aq \rightarrow \bar{e} \ aq^*$ mechanism it is necessary to have an accurate profile of the ground state behaviour of the hydrated electron, that is the decay of this species at high concentrations. Experiments were therefore designed to follow the formation and decay of the hydrated electron at radiation intensities a factor of 10^2 above those employed by Klein and Warner.

A accelerator
B control console
C plexicell
D laser
E lead screens
F flow system
G lead box
H photomultiplier
I lens, filter, iris
J junction box
K power supply to H
L oscilloscope
M copper buss bar,
    ground stake
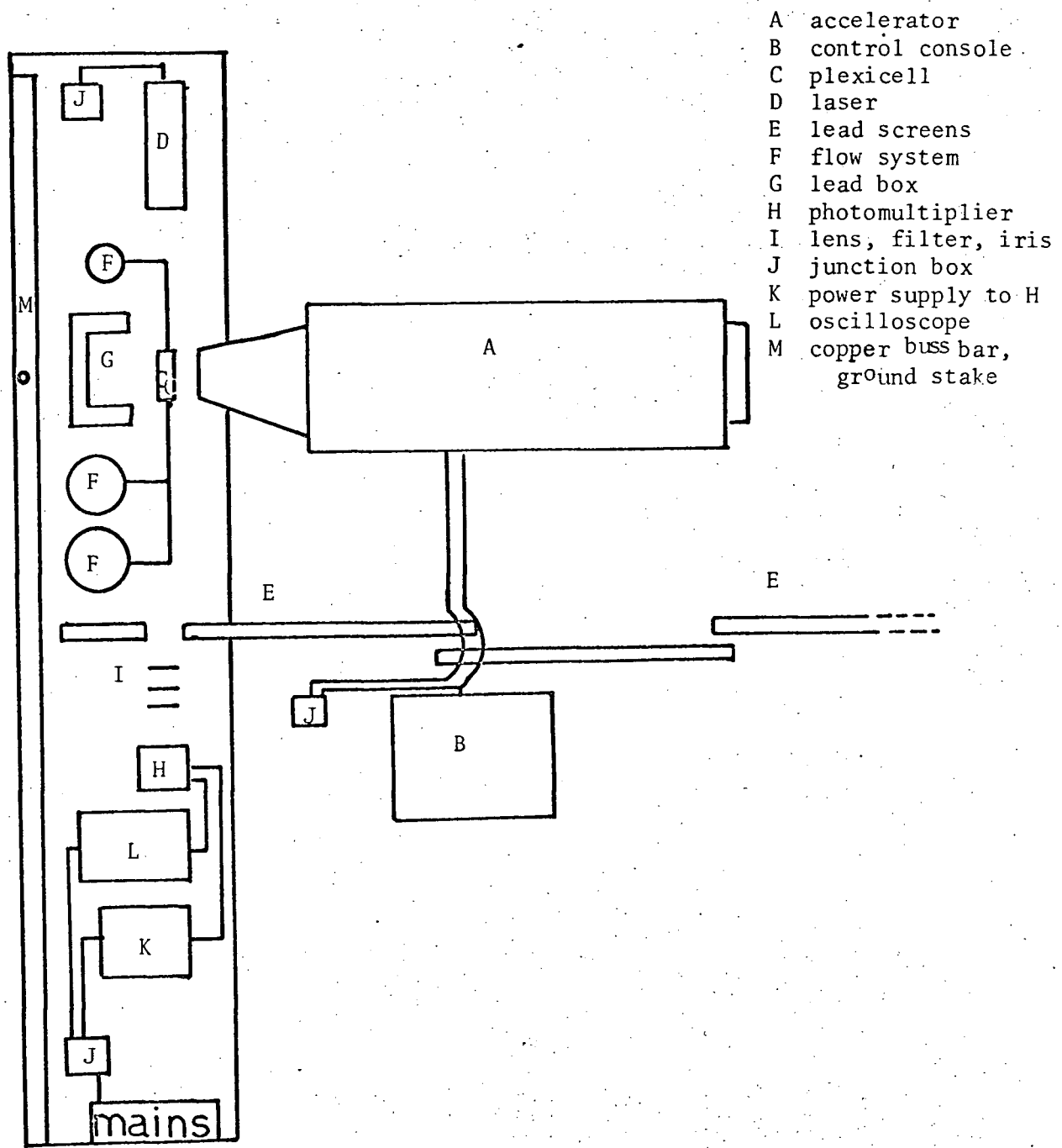
Diagram 6. The accelerator Laboratory

The Technique of Pulse Radiolysis, and Kinetic Spectroscopy

The formation and decay of the hydrated electron produced during the pulse radiolysis of aqueous media was followed by a kinetic spectrophotometric technique. A Helium-Neon laser was used as a monitoring light source and transient optical absorptions produced during and after the pulse were detected by a photomultiplier, displayed on an oscilloscope and photographed.

A schematic diagram of the accelerator laboratory in which these experiments were carried out is shown in diagram 6; details of the equipment are listed in the following sections and in diagrams 7, 8 and 9.

The Irradiation Cell

In designing the irradiation cell several important factors had to be considered:

(i) the window of the cell should be of suitable material and thickness to allow the maximum number of electrons in the pulsed beam to penetrate the solution.

(ii) If too deep a volume of solution is irradiated the electrons will penetrate to only a certain depth and thus space charges may appear.

(iii) It was necessary to remove the irradiated solution and replenish the cell quickly between the pulses.

(iv) A variable path length was desirable in view of the nature of the assumptions in relating charges in optical density to charges in the concentration of the absorbing specie.

(v) The width of the irradiation cell should be comparable to

the width of the laser beam in order to detect simultaneously events in call areas of the cell.

The final design of the irradiation cell in its supporting framework is shown in diagram 7. The support was constructed from 25 mm thick polished plexiglass and thus the irradiation cell has been called the plexicell. The plexicell is 11.2 mm in length and stands 10.4 mm high. An upper section of the plexiglass block was removed, the area of the resulting space being approximately that of the electron tube window in the accelerator. A hole was drilled through the remaining plexiglass either side of the space, into which a long thin glass tube could be inserted. A recess for an end window and a port were also machined at each end of the block as can be seen in the diagram.

The thin transparent 100 mm long glass tube of 1.5 mm internal diameter and 0.2 mm thick walls acted as the irradiation cell proper along which the laser beam was directed. (After several pulses the glass discoloured due to the presence of trapped electrons, and so the tubes were regularly replaced. To ensure uniformity in thickness and transparency in all the experiments a supply of KIMAX (U.S.A.) capillary tubes was purchased and the final specifications of the plexicell modified to fit these tubes.) The glass tube was retained firmly in position by a set of aluminium plates at both ends of the plexicell; these also supported the windows and their rubber backing discs ensured the cell to be water tight when a gentle pressure was applied to the plate screws.

The windows of the cell were polished 15 mm diameter pyrex discs. The glass tube reached to within 5 mm of either window; a smaller distance between them led to the trapping of gas bubbles often introduced in the
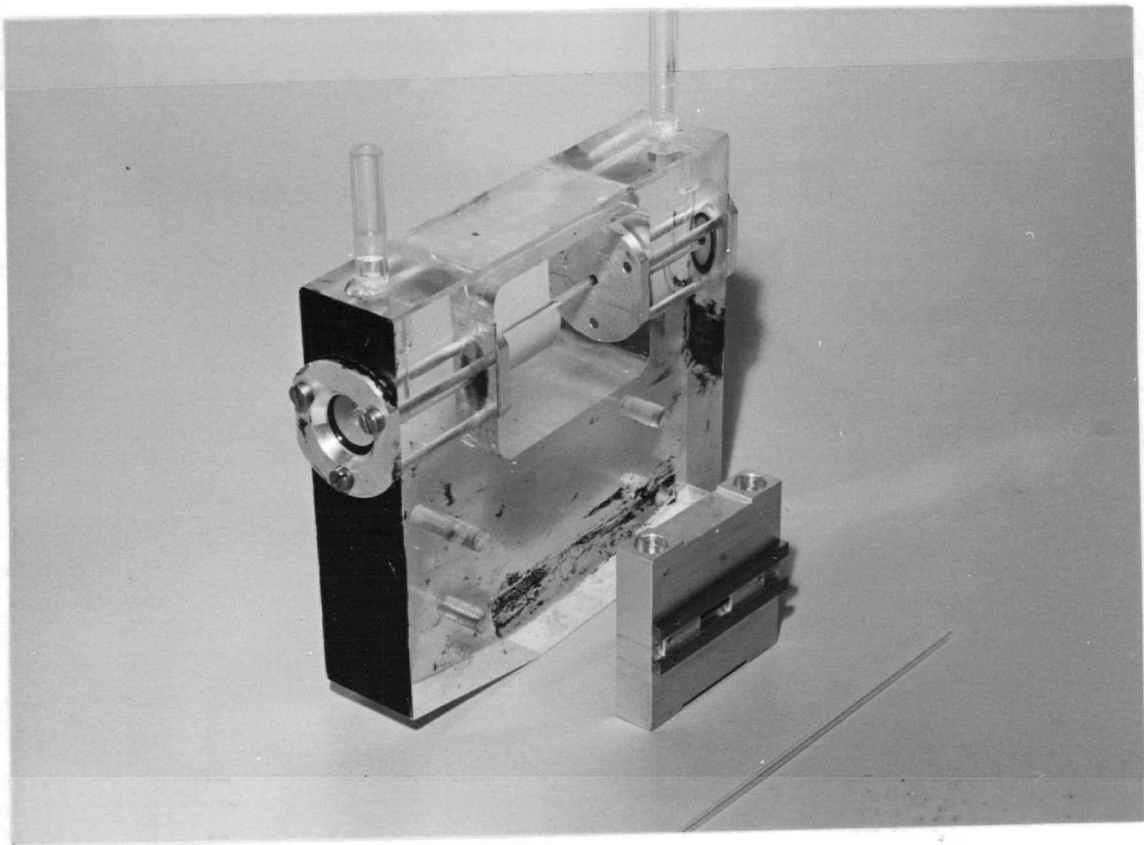
Diagram 7. The Plexicell and Components

flow of the sample solutions and otherwise easily removed. Fitted plexi-
glass ports of 6.7 mm diameter tapering to 2.5 mm diameter just above the
ends of the glass tube controlled the flow of solution through the plexicell.

A block of aluminium 9.6 mm thick and 4.5 mm by 4.1 mm high was
machined to fit into the empty section in the plexicell. The 20 mm by
1 mm wide slit cut along the centre of the block was aligned with the
glass tube, and two small doors of 0.8 mm aluminium slid along a recess
(in the block) facing the tube.

The aluminium block had a two-fold purpose. Firstly it represented
the variable path length for the irradiations as it was inserted on the front
side of the plexicell facing the accelerator. When the aluminium doors
were fully closed the total electron beam was absorbed by them. Secondly
the slit in the block served to collimate the electron beam. Previous
studies using the whole of the electron beam to irradiate the solutions
in the plexicell had shown some very curious variations in the light
intensity that completely masked the absorption signal under investigation.
The probable origin of these will be discussed briefly elsewhere, but
their elimination was only possible by restricting the electron beam to
an area comparable to the irradiation tube. For a while the restrictor
was a circular plate of 0.8 mm thick aluminium containing a slit of the
required path length that could be attached to the front face of the
accelerator. However this slit did not define the path length with
sufficient accuracy due to the undetermined divergence of the electrons
between the slit and the glass tube; the concentrations of $\bar{e}$ aq and
observed rate constants calculated from these early studies were to greatly
influence the design of later experiments.

Three holes drilled into the lower part of the plexicell permitted screw attachment of the cell directly to the front of the accelerator, or to a brass support (or the optical bench) on which the plexicell could be rotated in any direction. In all the experiments discussed here the plexicell was attached to the Febetron as this markedly reduced the high noise level on the signals recorded; the direct grounding of the cell when in contact with the machine and the reduced air space between the window of the electron tube and the irradiation cell probably both contributed to the improved signal to noise ratio.

The Electron Accelerator

In these experiments the source of high energy ionising radiation was a pulsed electron accelerator manufactured by Field Emission Corporation (Oregon). The Febetron which operates on the field emission principle produced single intense pulses of nanosecond duration of 0.5 MeV electrons.

In the initial stages of this work the Febetron model 701-2660 pulser and 5235 electron tube were employed to produce a 50 nanosecond pulse of 0.52 MeV electrons. The peak beam current observed at the window of this electron tube was 1000 amperes. The energy of the electrons in the pulse can be varied according to the D.C. charging voltage; the charging circuit of the Febetron operates on the Marx Surge Circuit principle. The impedance of the electron tube was fairly constant thus the beam current varied with the charging voltage. The beam current and pulse shape (with a half width of $\sim$20 nanoseconds) were reproducible to within a few percent ($\sigma = \pm 3\%$) under identical charging conditions.

At peak performance the Febetron gave a 50 nanosecond pulse of 0.52 MeV electrons amounting to a total deposition of energy of $\sim 10^{19}$ eV.

The majority of experiments were carried out with the 3 nanosecond pulse which was obtained by attaching the model 2770 pulse shortner to the Model 2660 pulser case and replacing the electron tube with a smaller model, no 5510. At peak performance this assembly gave a 3 nanosecond pulse of 0.5 MeV electrons and a beam current of ~ 1000 amperes. The total energy deposited was $\sim 10^{19}$ eV but the dose rate was increased to 5×10^{26} eV gram^{-1} sec^{-1} compared to 10^{26} eV gram^{-1} sec^{-1} with the long pulse. The reproducibility was within 5%, but with both electron tubes the greater the number of pulses in excess of the mean "lifetime" of the tube, the worse the reproducibility of their quoted characteristics. Typical pulse shapes are shown in figure 10a.

The electron beam current was measured with an apertured Faraday Cup shown in figure 10b. The cup contains a T & M Research Products Model GR-1-05 current viewing resistor (C.V.R.) with an impedance of 0.0507 ohms. The voltage pulse across the C.V.R. was fed into the vertical display of a Tektronix model 454 oscilloscope via doubly shielded RG58 coaxial cable coupled to a 50 ohm terminator at the input to the oscilloscope.

Solutions and Flow Techniques

Laboratory distilled water was redistilled from acidified potassium permangate solution and kept in a resevoir flask (built into the flow system) under an atmosphere of Helium gas. Solutions prepared containing other solutes were always made up from this supply of doubly distilled water.
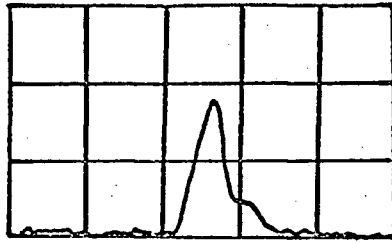
50 nsecs/div (horiz)
  typical pulsed
  wave forms observed
 from the electron irradiation
  tube.
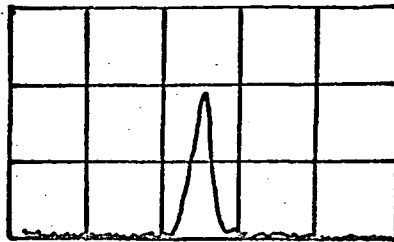
Diagram 10.

10 nsecs/div (horiz)

(a)
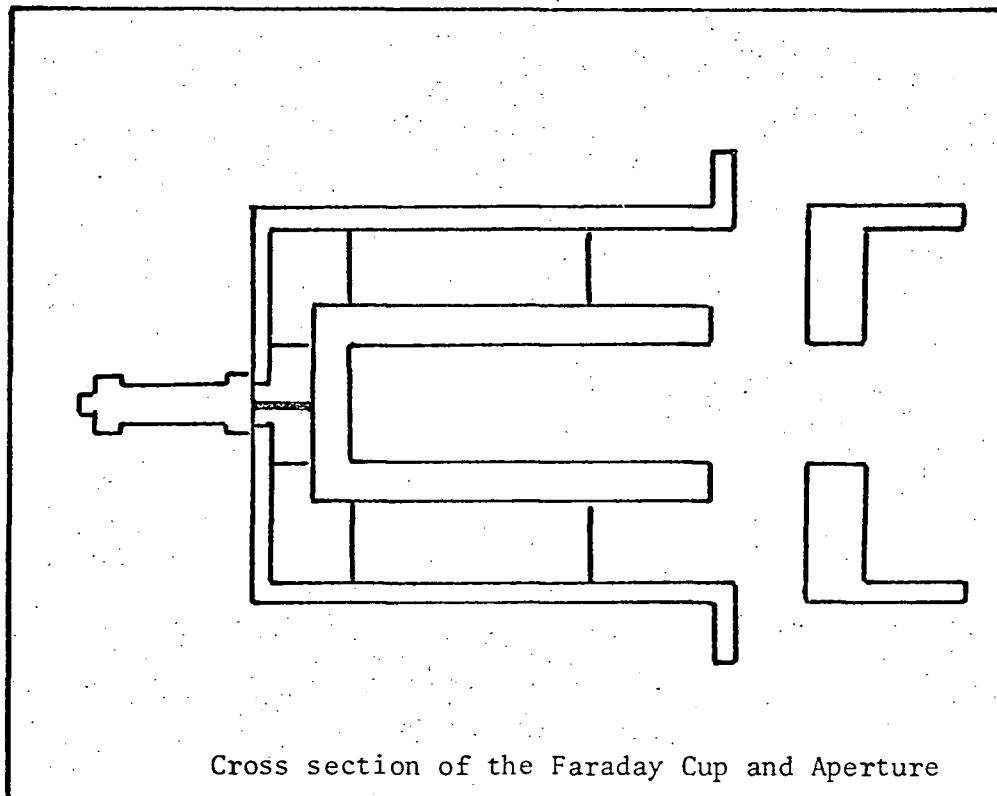
Cross section of the Faraday Cup and Aperture

(b)

The 0.26 M isopropyl alcohol solution was always freshly prepared from analar B.D.H. reagent without further purification. A supply of 0.0025 M and 0.1 M H_2SO_4 solutions were also made up from analar B.D.H. acid, and after degassing kept under an inert atmosphere of helium in a second resevoir flask in the flow system.

These resevoirs were 2 litre three necked flasks with individual flow lines to the irradiation cell that could be sealed when not in use. Each flask was connected to a common threeway stopcock which controlled the flow of helium gas through the flasks; an arrangement of traps and secondary stopcocks made improbable any accidental filling of the gas line with solution. Helium gas was bubbled vigorously through the solutions via a frittered glass oval to ensure efficient degassing; the oxygen content of the solutions was ∿1 ppm, i.e. that contained in the gas itself. The degassing took place for several hours when the resevoirs were completely refilled with fresh solutions, otherwise for 30 minutes before the experiments began. (When isopropyl alcohol solutions were used degassing was gentle and only for 10 minute periods due to the high vapour pressure of the alcohol.) During this time the helium escaped to the atmosphere through an open stopcock in the flask; the solution in the plexicell was replaced with a fresh volume of liquid by closing this stopcock, briefly pressurising the flask and then opening the appropriate flow line to the cell. The surplus liquid was collected through another line on the exit port of the cell that led into a residue flask. The temperature of all these solutions was 19° ±1°C.

Unless stated otherwise in the text the solution was replenished in the irradiation cell after each pulse. A pictureá : representation of the flow system is shown in diagram 11.
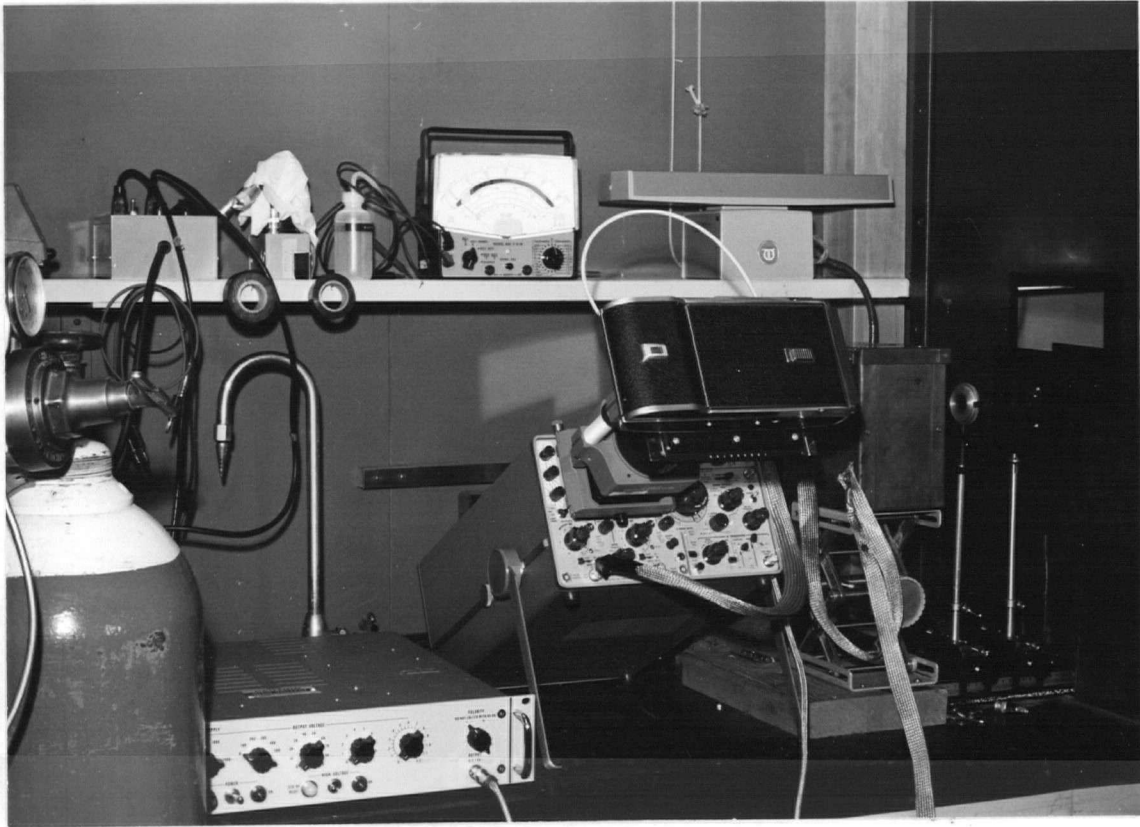
Diagram 8. The Electronic Detection System

The Detection System - Optical

The locations of the laser and photomultiplier with respect to the plexicell and the accelerator are shown in diagram 6.

(i) The laser

The analysing light source was a Spectra physics model 130C D.C. excited Helium-Neon laser, that emitted a continuous parallel beam at 6328Å. The beam width was 1.4 mm and the maximum output power 1 m watt. The intensity of the beam could be varied; the laser was operated under conditions of minimum "noise" which proved to be just below the maximum output power. The reason for this is given below.

Small irregularities on the inside of the plasma tube bore and the exit aperture tend to diffract some of the light away from the principal axis, and although the loss is so small as to not noticeably affect the power output, the intensity distribution of the beam varies with distance from the aperture. In this case the irradiation cell was 90 cm from the aperture and the intensity spread was still contained within 2 mm, the diameter of the glass irradiation tube; there was no appreciable loss of intensity as the beam passed through the solution but the diffraction was enhanced to a small extent. At the entrance to the photomultiplier box some 3 metres away the main beam was still 2 mm in diameter but the diffracted light was irregularly scattered about it. An adjustable non reflecting iris was mounted on the optical bench immediately before the focussing lens and in this way the scattered light was eliminated.

An inevitable degree of instability in the laser and 60 Hz fluctuations in the intensity from the main power lines were detected on

the photomultiplier and added to the "noise" on the absorption and decay

trace of the hydrated electron. It was possible as well to pick up

extremely fast and reproducible signals of ∿200 M Hz frequency and higher

in the laser beam. This was attributed to one of the additional

resonance frequencies in the oscillation as this laser does not operate

on a "single-mode" technique. The resonant frequencies are spaced f =

$\frac{c}{2L}$, $\frac{2c}{2L}$, $\frac{3c}{2L}$ ... where c = speed of light and L is the optical cavity

length. In this system the optical cavity length is ∿30 cm) which

could correspond to the high frequency observed. In addition these

frequencies are perturbed by small amounts according to how far the

resonance is from the centre of the Neon resonance and any slight changes

in the cavity length (due principally to thermal effects). These pertur-

bation frequencies can also be detected in the 1 K Hz to 100 K Hz range,

will be present simultaneously and are not in phase. As a result the

main signal from the laser on a wide-band oscilloscope has superimposed

noise like traces which only disappear when these cavity resonances

become symmetrical about the Neon resonance line and, through an apparent

self-phase locking, go to zero. The extent to which this ripple on the

laser signal interfered with the transient absorption signals is considered

in the results and discussion.

In the experiment designed to follow the formation of absorbing

species in different areas in the irradiation cell, the laser beam passed

along the whole tube as usual and the changes in intensity across the

diameter of the laser beam itself were monitored. This was done by align-

ing a thin brass restriction plate containing four pinholes of 0.031,

0.020, 0.0225 and 0.0135 (thousandths of an inch) bore parallel to the
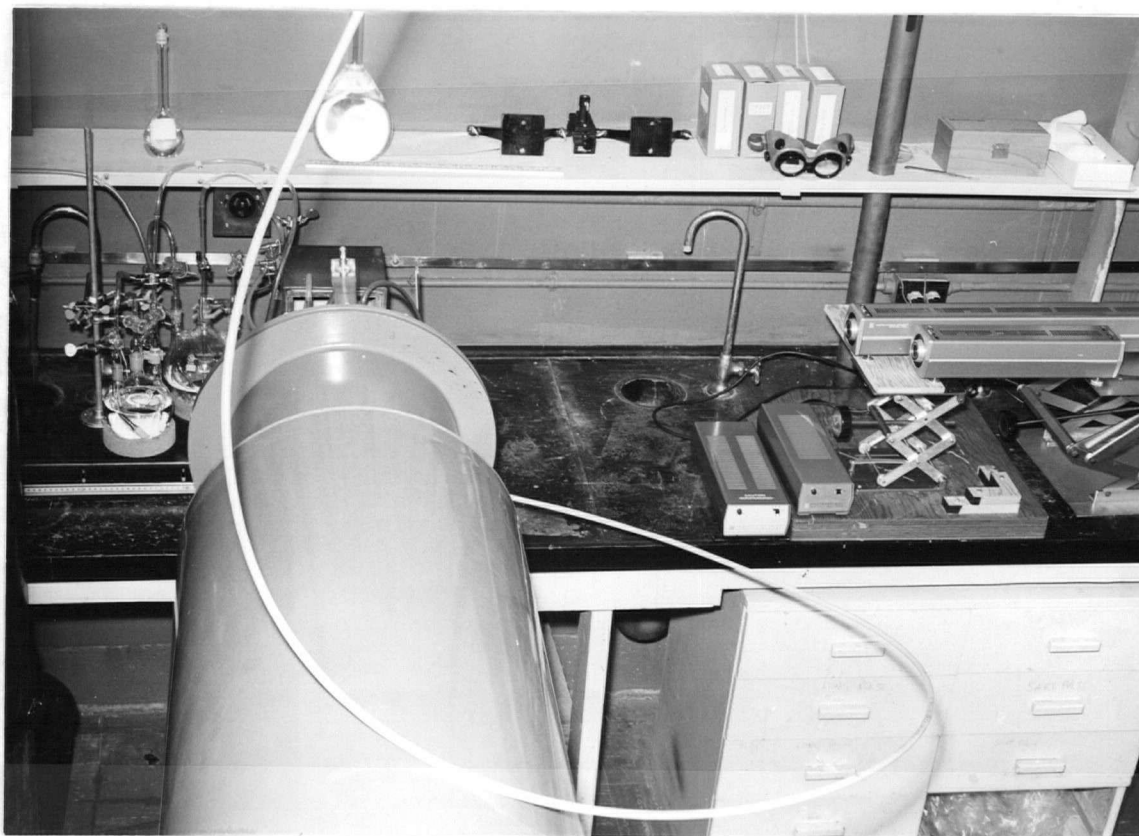
Diagram 9. Showing the apparatus in experimental positions

laser beam, in a position on the optical bench after the plexicell and
before the iris. The restriction plate was mounted on a stand which had
a fine lateral adjustment; thus the pinhole of choice could be moved
across the width of the laser beam and effectively "scan" the irradiation
cell.

(ii) Filters and Lenses

A 6328$\overset{\circ}{A}$ (Baird-Atomic Inc. interference type B11 with <10%
transmission outside the narrow band pass) filter that transmitted about
60% of the incident laser beam was incorporated into the optical arrange-
ments as shown in diagram 6. The reasons were twofold. The high intensity
Cerenkov emission occurs at all wavelengths and although the plexicell
had been blackened on its outer surfaces to prevent the reflection or
transmission of the Cerenkov light the cell windows were open and quite
transparent. It was not expected however to observe a significant intensity
at 90° to the electron beam. The second reason for using a red filter
concerns the relative sensitivity of the photomultiplier to different
wavelengths. The photomultiplier in use had a higher relative sensitivity
to shorter wavelengths with a maximum response at $\sim$3500$\overset{\circ}{A}$. A small
fluctuation in intensity at a low wavelength would correspond to a large
change in intensity in the red and might therefore falsify the height and
shape of the signal recorded.

The neutral density filters used periodically to test the
linearity of the system were 1% and 10%. These were Baird-Atomic inter-
ference filters.

Complete absorption of the laser beam gave a signal of only
$\sim$25 mv from the photomultiplier operating at 550 volts. The details of
the electronic detection system are given later together with the reasons

for this small signal. Ultimately the best signal to noise ratio (set
by the limits of the maximum permissible gain in the photomultiplier and
the noise observed at higher operating voltages used to amplify the small
signal) was obtained by focusing the laser beam onto the photocathode.
A 8.5 mm focal length polished quartz lens was mounted on a support
capable of fine lateral and vertical adjustment and orientated to give
the best possible signal from the laser beam. Normally readjustment was
unnecessary as the geometry of all the equipment was reproducible even
after any displacement or modifications to the system.

The Detection System - Electronic

(i)   The photomultiplier

A R.C.A. Victor 1P28 photomultiplier with a S5 spectral response
and a 100 ohm load resistance was used to follow the variations in the
intensity of the transmitted laser beam. The load resistance and resistors
in the dynode chain were fitted into a compact metal base and the whole
assembly was housed in a copper box 19 cm high by 12 cm by 17 cm that had
been lined with ¼" thick lead (to protect the photomultiplier from X-
radiation). The lid of the box contained eight small holes that provided
a minimum amount of ventilation but because of the actual position of the
phototube no diffuse light could be picked up and amplified with the signal.
The ambient temperature in the box rose appreciably after prolonged use
of the photomultiplier and therefore the duration of experiments was kept
within a reasonable time and the photomultiplier periodically checked for
any marked increase in dark current. A modification to the housing to provide
a constant temperature cooling system has been designed and will be in use
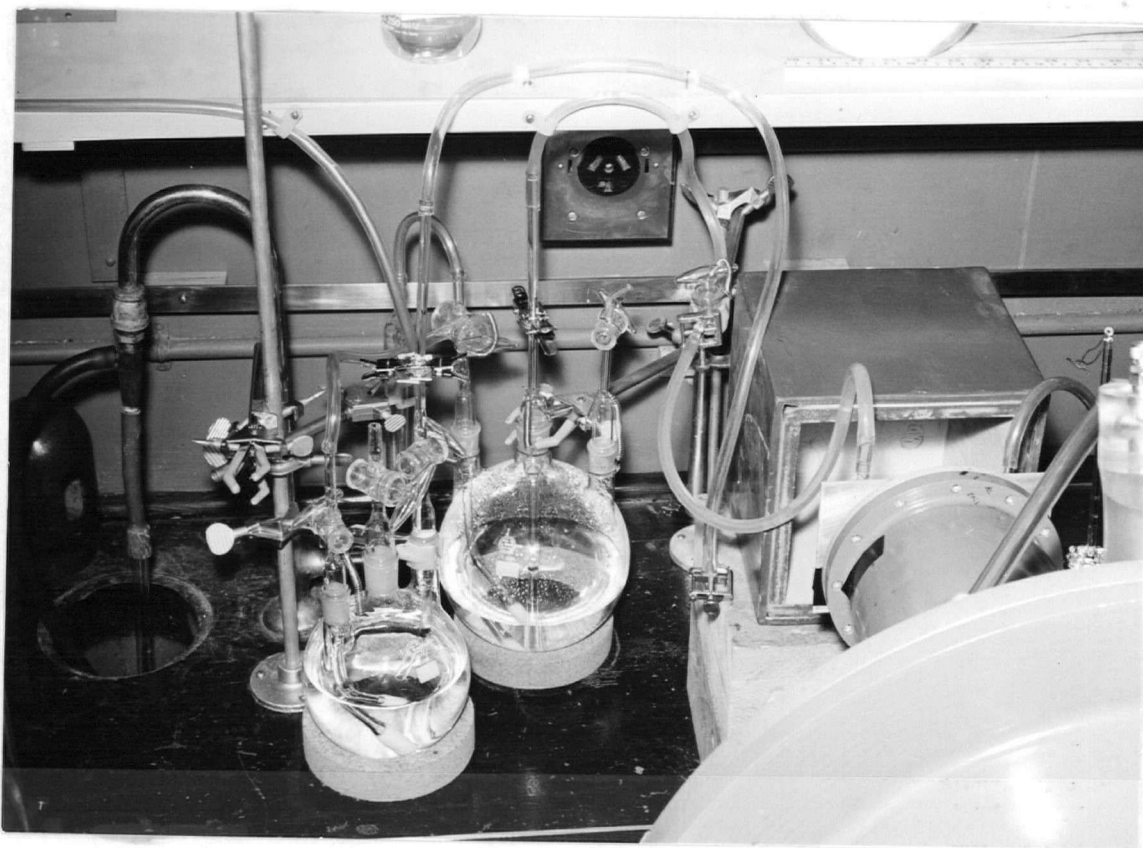
Diagram 11. The Flow System

for the next experiments in this project. Under the present conditions the temperature inside the copper box was 21° ±1°C.

A pinhole of 1.5 mm diameter was drilled through the front face of the shielding box thus allowing light focused through the pinhole to fall on to the photocathode. Between experiments the photocathode was protected from the laser beam by covering the pinhole.

The 1P28 has fast time resolution characteristics the anode pulse rise time of 10^{-8} seconds and time spread of 2×10^{-9} seconds at the voltages employed. The minimum length of RG71/B/U coaxial cable (used to match impedance with the load resistance) necessary to transmit the signal to the oscilloscope was 18"; the cable was doubly shielded and fed the signal through a 93 ohm Tektronix terminator into the vertical amplifier input of the oscilloscope.

The maximum current that the dynode chain could sustain was 10 m amps but to avoid saturation effects and problems of non linearity in the response of the photomultiplier tube a working voltage of 550 volts from a power supply (5.5 mA D.C. across the chain) was normally used and the signals attenuated on the oscilloscope. For very small variations in intensity of the laser beam and the "pinhole experiments" the voltage was raised to a maximum of 750 V. At very low voltages i.e. low current along the dynode resistor chain, fluctuations in the dynode voltages con-tributed towards the non-linear behaviour of the tube; at voltages above 750 V the level of the noise on the signal, which had contributions from dark currents in the tube, amplified laser ripple, and feedback effects was unacceptable. In addition during the experiments there were adverse changes in the dark current and noise pulses due to the intense ionising

radiation and fields generated by the electron pulse. However these effects were reduced to as low a limit as possible by the lead screening in the copper box, the radiation shields and the double shielding on all the transmission lines, although this level was by no means completely satisfactory.

The photomultiplier was powered by a Fluke model 412B high voltage D.C. power supply whose output was stabilised to within ±0.005% per hour or ±0.02% per day's operation. The power supply was connected to the photomultiplier with coaxial doubly shielded transmission cable.

(ii)   Oscilloscope and camera

The Tektronix model 454 wide band path oscilloscope was used to display the variations in the intensity of the laser beam (i.e. the change in anode current across the load resistance in the photomultipler) during and after the electron pulse from the accelerator as a time dependent voltage signal. The rise time of the oscilloscope under these conditions was 2.6 nanoseconds.

The input power line from the mains 110 volts supply was filtered through a radiofrequency line filter attached to the back of the oscilloscope. As already mentioned the signal from the photomultiplier was terminated with 93 ohms at the input on channel 1 of the oscilloscope. The trace on the screen was trigged by an A.C. positive fluctuation in the signal and all low frequency signals were rejected. In each experiment the 100% light level was recorded immediately after the pulse by manually chopping the laser beam (at approximately 1 K Hz) and recording the rise of the signal and subsequent fall to 100% transmission again.

A Tektronix Type C-40 (polaroid) camera supplied with attachments for the oscilloscope was used to record the traces on polaroid polascope type 410 film which is particularly suitable for extra-high speed (rated as 10,000 ASA equivalent) photography and low level light sources such as the trace intensities available with the fastest sweeprate on the oscilloscope.

The Grounding System

It was imperative to have a good high frequency grounding system with all the equipment grounded effectively to one point as otherwise the intense magnetic and electric fields produced by the accelerator during the electron pulse completely interfered with any measurements. The power supply, oscilloscope and photomultiplier were all grounded to one another through the outer shielding on the doubly shielded coaxial cable. However it also appeared necessary to ground the noise filter on the oscilloscope separately, to take a ground lead from the photomultiplier box to the "common" ground point and to remove all the equipment from the mains earth by floating the plugs in a common junction box. It is probably more informative to illustrate the complete grounding scheme in a diagram (see diagram 12). The ground stake was attached to a long copper bar to which individual grounding tapes were bolted.

During the experiments it was discovered that many of the long thick grounding tapes and unshielded cables were merely acting as attennae, so all grounding tapes were kept to a minimal size and no cable remained unshielded.

The laser was also attached to a floating plug and grounded then

A accelerator
B control console
C plexicell
D laser
E lead screens
H photomultiplier
L oscilloscope
K power supply to H
M copper buss bar,
       ground stake

M

C

A

E

E

B

H

L

K

mains
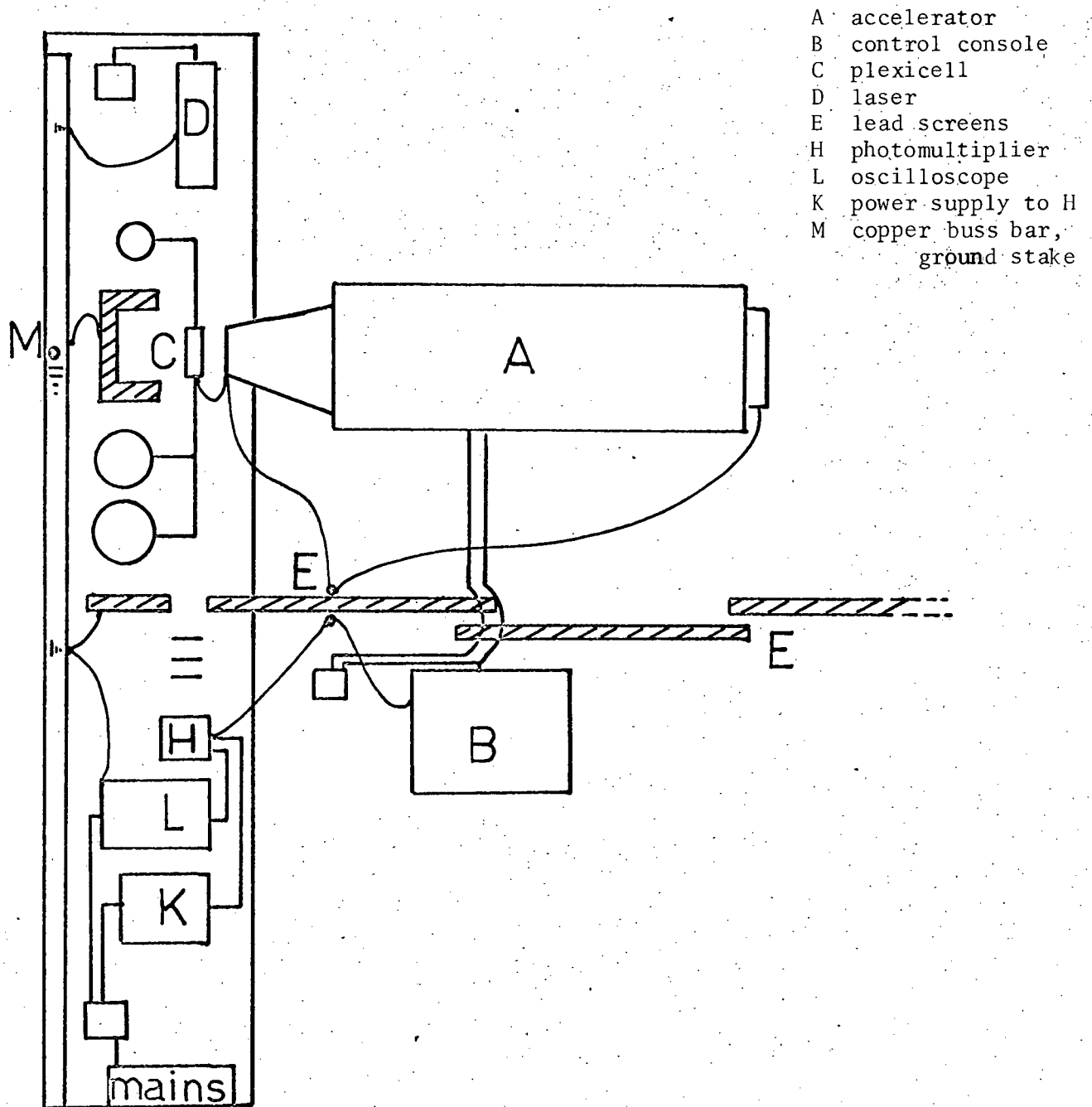
Diagram 12. The Grounding System

to the copper bar approximately three feet from the grounding stake. A piece of ¼" lead was folded around the side of the laser near to the accelerator to prevent any adverse effects on the laser output and ripple. There was a three-sided lead box immediately behind the plexicell which in the absence of the cell or other attachment on the front of the accelerator acted as a sink for the radiation produced.

As the alignment of the laser, plexicell, focusing lens and photomultiplier was critical, any vibration of these pieces of equipment markedly affected the signal, and often heavy "noise" on the signal could be tracked back to imperfect alignment. The other factors to consider were the occurrence of ground loops from doubly grounding some of the electronic equipment and the inevitable pickup from the mains of high frequency signals from machines in nearby laboratories.

The Computation of Data and the Results

The Input Data

This consisted of the recorded absorption signal as a function
of time during the decay of the hydrated electron. The measurements
were made on the photographs of the oscilloscope traces using a Micro-
scale with 0.1 mm divisions, and reasonable estimate was possible for
the next decimal place. A typical initial absorption signal would be
14.8 ± .05 mm (for a 2.5 mm path length) decreasing to ~10 mm after
150 nanoseconds, with a maximum possible absorption corresponding to
30 mm. Measurements were made every 5, 10 or 20 nanoseconds the time
interval depending on the sweeprate of the oscilloscope, and sometimes
estimates of the true height of the signal had to be made due to the
noise level. Because of this uncertainty after 100 or 200 nanoseconds,
it was often difficult to determine anything but an approximate half
life for $\bar{e}$ aq under the experimental conditions and therefore a comparison
has been made between the different results that relates the % decrease
in the absorption signal at a given time after the pulse. In those traces
where the noise and laser interference (see section II) were more than
an annoying width on the signal the $\bar{e}$ aq decay was not analysed. Attempts
were made to enlarge the polaroid photographs into both negatives and
prints for easier working but the inevitable distortions in the scale
and on the trace although small were sufficient to outweigh any visual
advantages.

Computation of Data

The analysis of the results collected in the long pulse (50 Nsec)
experiments indicated that the data could not be simply matched to

either a first or second order kinetic treatment. In addition the
duration of the pulse meant that the hydrated electrons were reacting
before the electron pulse (and thus the formation of the hydrated
electrons) was finished. With the short (3 Nsec) electron pulse
the latter problem was insignificant but the kinetics were not simplified.
The results from these experiments were therefore considered from three
independent approaches, covering the different mechanisms feasible in
this system.

(i) Two significant simultaneous processes occurring immediately
after the pulse.

(ii) One significant process only occurring after the pulse.

(iii) Two significant processes occurring consecutively after
the pulse.

Let x be the absorbing specie (ie. the hydrated electron) and
y any other specie subsequently formed in the system in significant
concentrations; k_1 is a first order rate constant and k_2 a second order
rate constant.

(i) If several processes are occurring simultaneously an
expression can be derived relating the change in concentration of x to
these reaction rates and the concentrations of any other species involved.
From an initial study of the data it was clear that if there were two
simultaneous processes in this system they would be first and second
order type reactions and so the following equation describes this case:

$$-\frac{d[x]}{dt} = k_1[x] + k_2[x]^2 \qquad \text{(or } k_2xy)$$

$$-\frac{1}{[x]} \cdot \frac{d[x]}{dt} = k_1 + k_2[x] \qquad \text{which on rearrangement shows that a}$$

plot of $\frac{1}{[x]} \frac{d[x]}{dt}$ against [x] should give a straight line of slope - k_2

and intercept k_1. A further rearrangement gives mathematically identical
plot but an interesting check on the way the data fits the treatment.

$$\frac{-d\ln x}{dt} = k_1 + k_2[x]$$

In the event of only one process occuring the appropriate k
will become insignificant and the term will equate to zero. The para-
meters evaluated from these plots were then fitted to a third degree
polynomial.

The assumption that optical density could be linearly related
to the concentration of the absorbing specie

$$O.D. = c. \varepsilon l \qquad\qquad \varepsilon \text{ extinction coefficient}$$

$$l \text{ path length in cms.}$$

was investigated experimentally and the results will be discussed later.

The optical density was considered as the variable, and the
two expressions below used to separate the two simultaneous processes

$$\frac{-1}{O.D.} \quad \frac{d\, O.D.}{dt} = k_1 + k_2 \frac{O.D.}{\varepsilon l}$$

$$\frac{-d\ln O.D.}{dt} = k_1 + k_2 \frac{O.D.}{\varepsilon l}$$

up to 200 Nseconds after the pulse.

(ii) If there were only one significant process occurring then
a detailed graphical analysis of the changes in optical density (in the
first 100 Nseconds or so after the pulse) should indicate the reaction
order.

First order process: $\ln x = k_1 \tau + \text{constant}$

A plot of $\ln \frac{(O.D.)}{\varepsilon l}$ against $\underline{t}$ should give a straight line of slope k_1.

Second order process: $\frac{1}{x} = k_2 \tau + \text{constant}$

A plot of $\frac{1}{O.D.}$ against τ should give a straight line of slope $\frac{k_2}{\varepsilon l}$. The

k_2 value was calculated from $\dfrac{1}{O.\overline{D}._\tau} - \dfrac{1}{O.D._o} = \dfrac{k_2\tau}{\varepsilon\ell}$

(iii)   If the mode of decay of the hydrated electron changes after a certain time and, for example, both first and second order processes are involved in sequence, then the behaviour of the specie still may be specifically classified before and after the transition period.   Here one must also include the possibility that the two mechanisms are of the same reaction order but occur with significantly different rate constants.   Any changes in the slopes observed from the treatment in (ii) should occur at approximately the same time after the pulse and in the same direction.

The underlying assumption in these approaches is that classical kinetic theory can be used to describe the behaviour of a system whose principal active specie has been consumed by the products of its own initial reactions in about 200 nanoseconds, and can be scavenged by additives of suitable concentrations in only a few nanoseconds.

The data was fed into a computer; the least-squares-fit programme containing the treatments for (i) and (ii) was also designed to provide information for (iii) by systematically eliminating the data points up to a given time after the pulse and recording the variations in the rate constants and the quality of the fit.*

All the long pulse data had been analysed assuming (ii) and it was from these graphs that the first apparent k_1 and k_2 values were calculated; these were a good indication of the order of magnitude to expect on the short pulse data some of which was also analysed in this

---

way as a precaution against errors in the input data or computer programme.

The results of each of the series of experiments will now be given in relation to the three treatments.

Variations of optical density with path length

Path lengths of 1.0 mm, 1.5 mm, 2.7 mm, 3.5 mm, 5.0 mm and 5.5 mm were used. When it became clear that the larger path lengths were giving rise to optical densities (O.D.) that deviated from the anticipated values (derivatives from Beer's law) then attempts were made to look at O.D. at even shorter path lengths. However the technical problems associated with the detection and amplification of the signal prevented such experiments. Two possible reasons for this deviation are (a) the effective path length of absorbing species was greater than the width of the slits due to an undetermined divergence of the electron beam, a more significant error at longer path lengths; and (b) the radial distribution of the electron beam itself is such that if the centre point of the slits did not coincide with that of the electron beam then there may be different numbers of absorbing species along the path length, arising from a spatial variation in the energy deposited in the medium.

The data is summarised in diagram 13. The variations in O.D. observed at the same path length may be in part due to (b) above and also to the fact that recently fluctuations in the output of the electron accelerator have been observed in this laboratory. The energy of the electron beam varied with the actual charging conditions of the accelerator and the time interval between pulses to a more significant degree than the manufacturers claimed. The pulse to pulse reproducibility
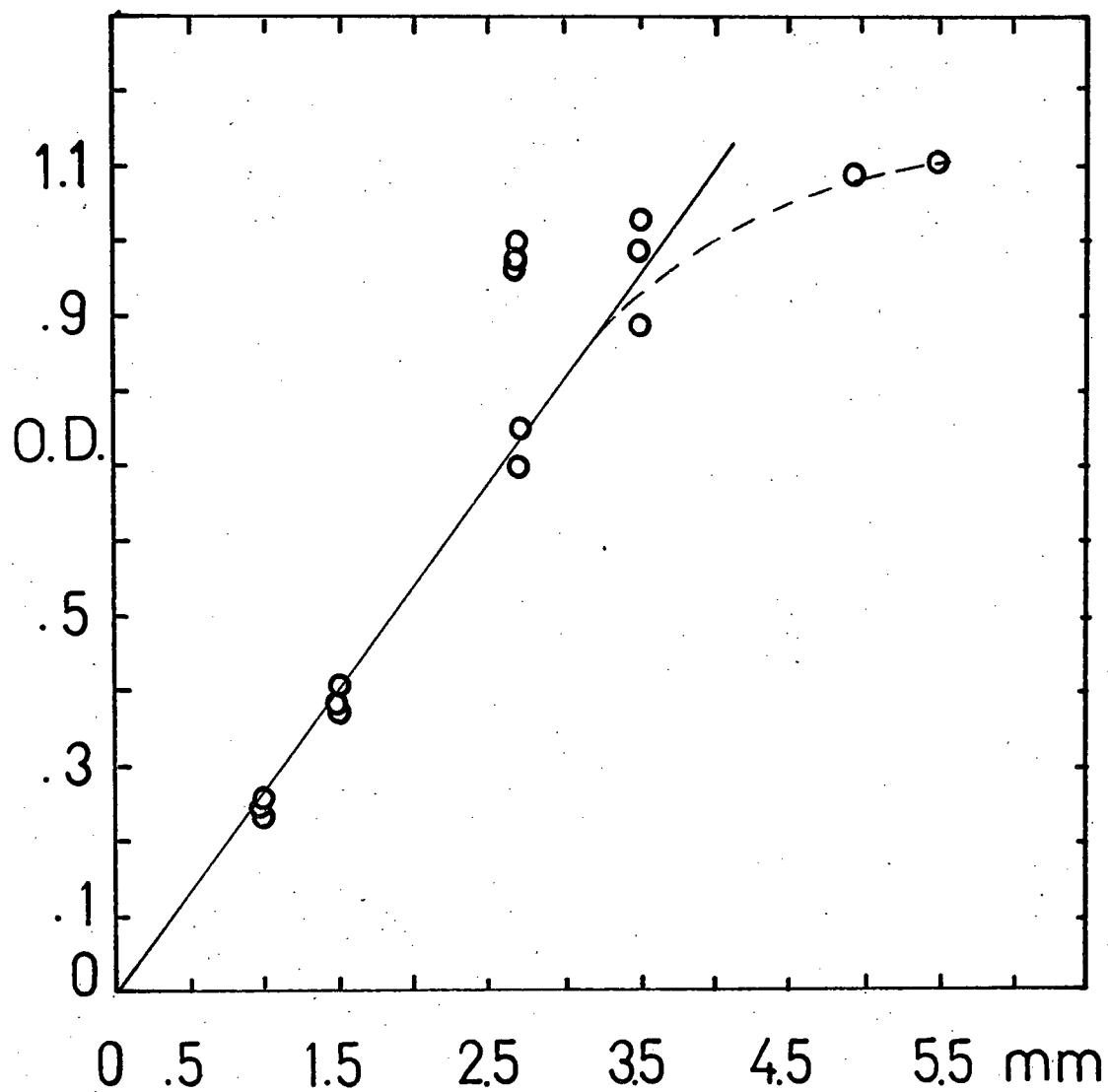
Diagram 13. Optical density as a function of path length

has now been improved by changing all the nitrogen gas in the high pressure chambers to oxygen.

The formation and decay of $\bar{e}$ aq after a 3 Nsec electron pulse

This section refers to the data collected on the decay of $\bar{e}$ aq after a single electron pulse at different path lengths. Some typical plots are given in diagrams 14, 15,16 which show the first and second order treatments and the apparent transition from one to the other at about 80 ± 10 nanoseconds in each case. Unimolecular and bimolecular decay processes might have been occurring simultaneously with one mode dominating the other at different times after the pulse, but none of the data fitted treatment (i). In some cases the transition period in the first order plots was then followed by a long linear portion which might itself be indicative of another first order decay occurring at a different rate. The slope of this line was linear to about 150 nanoseconds and gave a rate constant slower by a factor of 3.

The rate of decay of $\bar{e}$ aq was first tabulated from those experiments in which it had been possible to collect data every 10 nanoseconds and in most cases every 5 nanoseconds. The average value for the first order rate constant k_1 as calculated from a plot of $\log \frac{(O.D.)}{\varepsilon \ell}$ against time was $8.80 \pm .8 \times 10^6$ sec^{-1}. With data taken in other experiments only every 20 nanoseconds there were not as many points on the graph up to the 80 nanosecond transition period and it was apparent that this average k_1 value was slightly lower, viz. $5.7 \pm .8 \times 10^6$ sec^{-1}.

The plots of $\frac{1}{O.\bar{D}.}$ against time were linear after about 80 nanoseconds in all the experiments, and irrespective of the time intervals in which the data was collected the values for k_2 were in reasonable
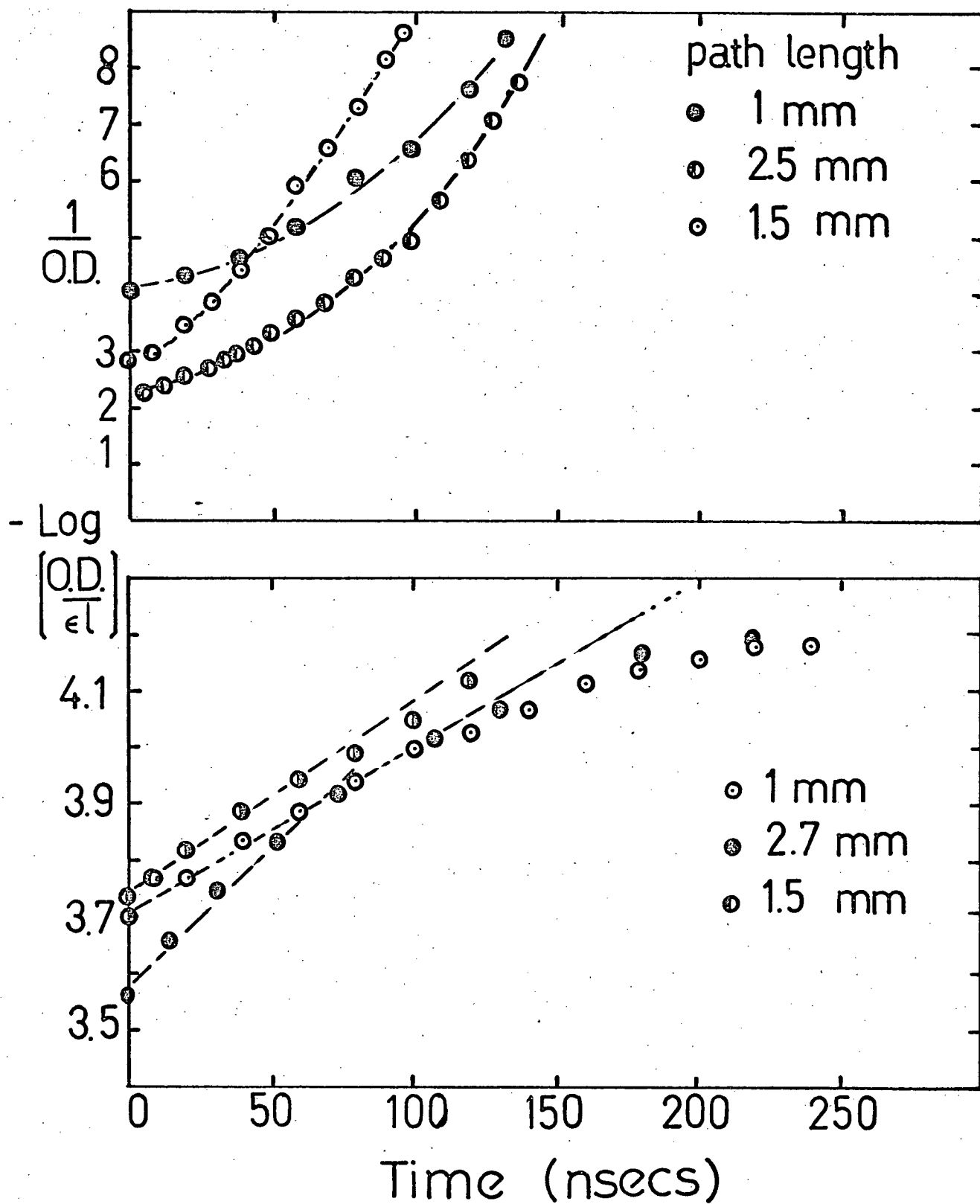
Diagram 14. Some first and second order plots for the decay of the hydrated electron
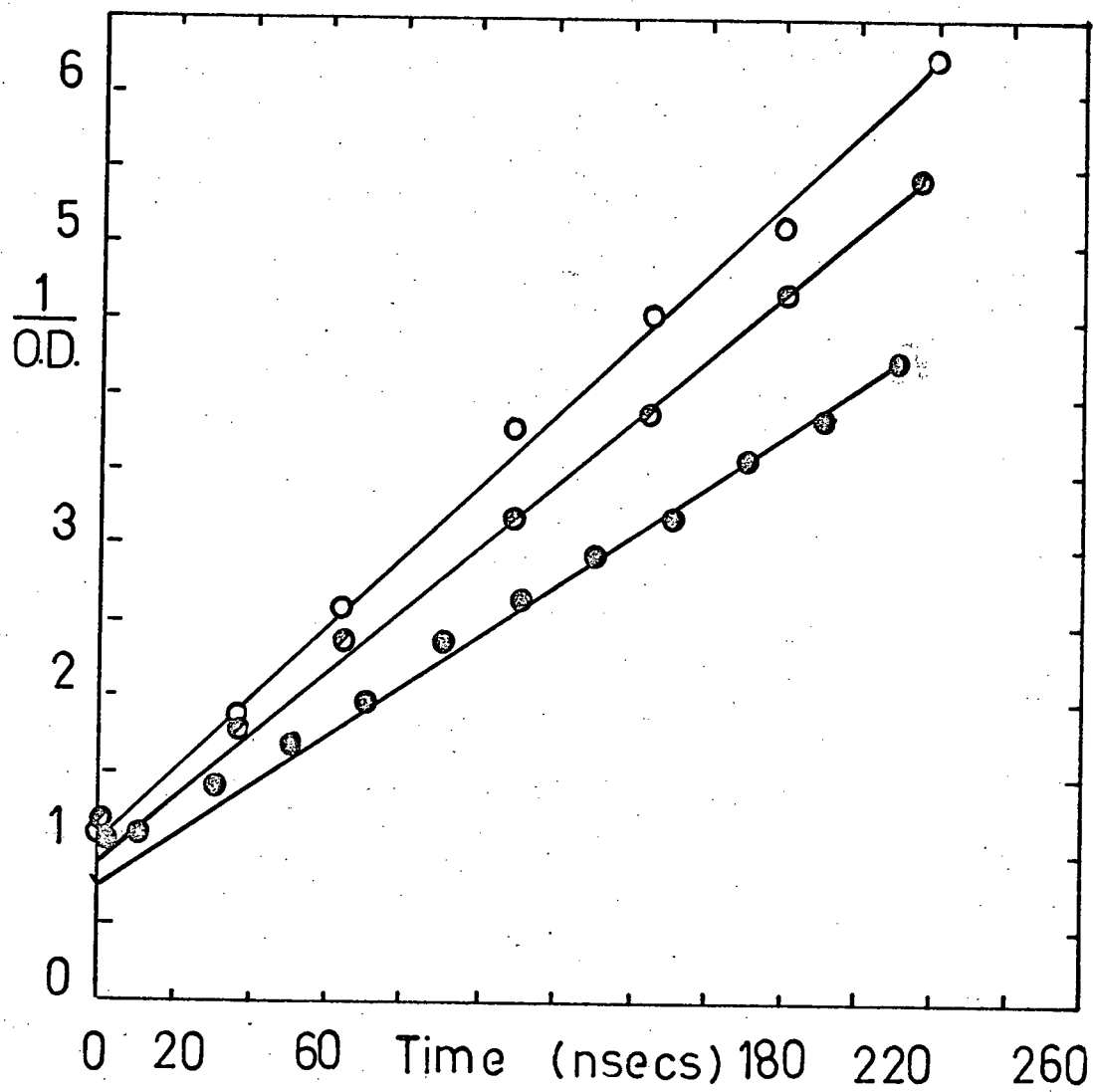
Diagram 16. Second order plots for the decay of $\overline{e}$ aq.

agreement with an average value of $5.88 \pm 1.2 \times 10^{10}$ M^{-1} sec^{-1}.

Individual experimental results are compared in Table (III)

Table III

path length cm	k_1 10^{-6} sec^{-1}	k_2 10^{-10} M^{-1} sec^{-1}
Data every 5, 10 nanoseconds		
0.1	7.17 ± .15	4.49 ± .07
0.15	8.38 ± .02	6.45 ± .23
0.15	8.26 ± .13	6.11 ± .11
0.35	9.56 ± .54	6.00 ± .42
0.55	8.19 ± .07	insufficient data
0.55	8.19 ± .09	insufficient data
Data every 20 nanoseconds or longer		
0.1	6.72 ± .14	4.25 ± .23
0.1	5.73 ± .42	4.14 ± .09
0.1	5.18 ± .29	5.23 ± .26
0.27	4.92 ± .02	8.20 ± .33
0.27	6.06 ± .00	6.60 ± .11
0.27	insufficient data	7.49 ± .29
0.55	5.30 ± .45	insufficient data

The evidence strongly suggests that for the first 80 nanoseconds at least the $\bar{e}$ aq decays in a 1st order process; this is a puzzling concept in view of the generally accepted bimolecular nature of the decay of $\bar{e}$ aq in irradiated neutral water. After this period there appears to be a transition to 2nd order behaviour which holds over several halflives. The apparent linearity of some first order plots after 80 and up to about 150 nanoseconds with an average k_1 value of $2.62 \pm 1 \times$

$\bar{e}_{aq}$, 1 pulse.

20 mV/div.

100 nsecs/div.

$\bar{e}_d$, 2 pulses.

50 mV/div.
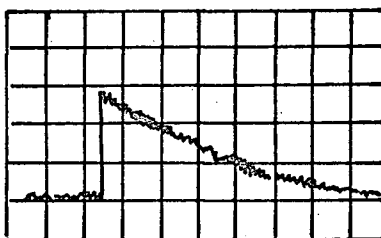
50 nsecs/div.

$\bar{e}_{aq} + H^+$.

10 mV/div.
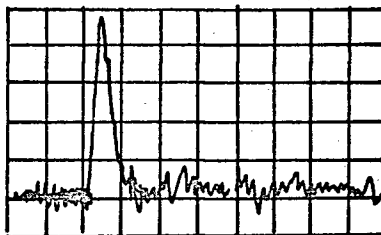
50 nsecs/div.

$\bar{e}_{aq} + R\text{-}OH$.

20 mV/div.
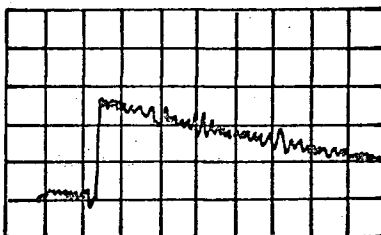
50 nsecs/div.

Diagram 15 (b). Oscilloscope traces showing the $\bar{e}$ aq decay in the presence of different solutes.

10^6 sec^{-1} may or may not be a real effect: this might simply be the beginning of a very long slow curve which would only be noticed if data up to several hundred nanoseconds could be taken at small time intervals. The level of noise (that masked the absorption signal) on the traces was too great to permit accurate measurements up to this stage.

Formation and decay of $\bar{e}$ aq after a 50 Nsec electron pulse

These experiments were carried out in a different laboratory but with essentially the same equipment. The important differences are the length of the pulse, during which time the $\bar{e}$ aq is formed and begins to decay and may possibly reach a steady state concentration, and the path length of the cell which was always 7 mm.

The decay of $\bar{e}$ aq was shown to follow first order kinetics over about 100 nanoseconds, and a halflife of about 130 nanoseconds. The rate constants are given as

$$k_1 = 1.91 \pm .07 \times 10^7 \text{ sec}^{-1}$$
$$k_2 = \sim 10^{11} \text{ M}^{-1} \text{ sec}^{-1}$$

The effects of multiple pulsing

The decay of $\bar{e}$ aq was bimolecular after several pulses and the rates increased significantly. Although some first order character was still evident in the data after three or four pulses the increase in rates was such as to indicate pseudo first order behaviour in the presence of relatively high concentrations of radiolytic products. The average halflife of [$\bar{e}$ aq] was reduced by about a factor of 2 after

$k_1 \times 10^{-6} \text{ sec}^{-1}$

$k_2 \times 10^{-10} \text{ M}^{-1} \text{ sec}^{-1}$
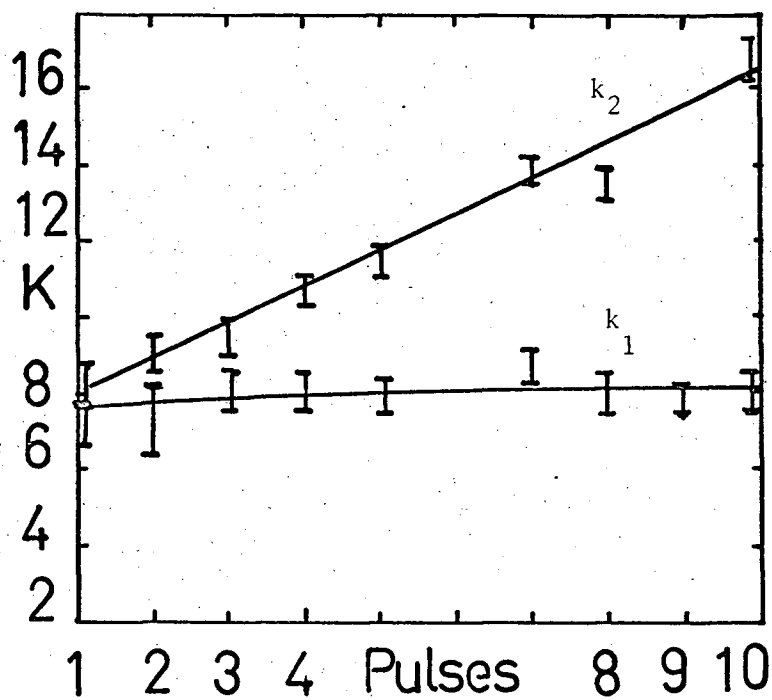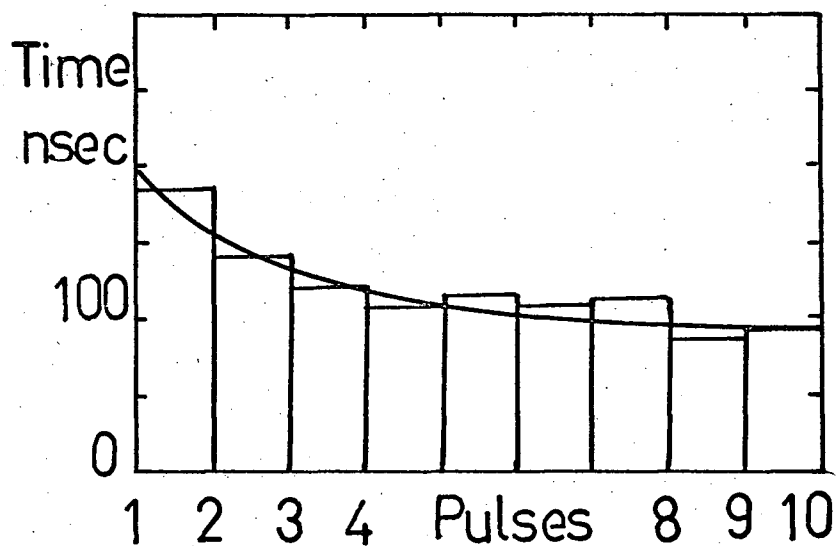
Diagram 17. (a) The effects of multiple pulsing on (a) rate constants k_1 and k_2, and (b) time taken for the initial absorption signal to to reduce by a factor of 2

10 pulses. A typical plot from a multiple-pulse experiment is shown

in diagram 17 where the relative changes in k_1 and k_2, and the halflife

of $\bar{e}$ aq are included as a function of the number of pulses for two

different path lengths, 1.0 mm and 2.6 mm.

The Effect of H^+

The addition of acid to the aqueous system markedly reduced

the lifetime of the hydrated electron. With a path length of 3.6 mm

and 5×10^{-3} M H^+ from sulphuric acid the absorption signal had disappeared

in about 40 nanoseconds (whereas the neutral water control indicated only

a 17.5% decrease during the same time interval).

From the points available for the $\bar{e}$ aq decay in acid solution

the reaction was unambiguously first order; this is explained as the

concentration of H^+ exceeds that of $\bar{e}$ aq (as calculated from the initial

optical density) by 10^2 and thus pseudo first order kinetics might be

anticipated.

$$\bar{e} \text{ aq} + H^+ \longrightarrow H + OH \text{ aq}$$
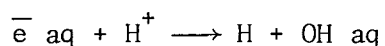
The rate constant was calculated to be $7.4 \pm .5 \times 10^7$ sec^{-1}. The

control sample data showed a first order decay ($k = 9.46 \pm .16 \times 10^6$ sec^{-1})

up to about 80 nanoseconds and then a second order process appeared to

take over. The probable reasons for this effect commonly seen in

neutral water will be discussed in part IV.

The effect of an alcohol

Isopropyl alcohol reacts readily with OH and H radicals and

therefore should increase the lifetime of the hydrated electron.

Whereas in the control sample the initial absorption signal had decreased by 42% 100 Nsecs after the electron pulse, the signal from the alcoholic solution had only decreased by 20%. Again data from the control sample fitted a first order treatment up to about 75 nano-seconds. The data from the alcohol experiments gave good second order plots over the complete time period examined (140 nanoseconds) and with one exception the first order treatments could be ignored. The reasons for the exception are not known -- the points were not scattered.

In treatment (i) although the fits were not satisfactory the evaluated rate constants were of the correct order of magnitude. The k_2 calculated from treatment (ii) was $3.8 \pm .1 \times 10^{10}$ M sec^{-1}.

The effect of oxygen

The variation in the rate of decay of $\bar{e}$ aq in the presence of different concentrations of dissolved oxygen was followed during three series of experiments; the first series used liquid water containing "atmospheric" oxygen (1/5 atmos), the second employed oxygen saturated solutions (1 atmos) and the third a control solution degassed in the usual manner. A 3.6 mm path length was used. The data from the decay of $\bar{e}$ aq in the control solution initially fitted a 1° order treatment to about 90 nanoseconds and the decay in the oxygen saturated solutions followed the same pattern. It is suggested that pseudo first order kinetics are given in the latter case because of the much higher concentration of oxygen in relation to the hydrated electron. The atmospheric oxygen samples supported a second order decay for the hydrated
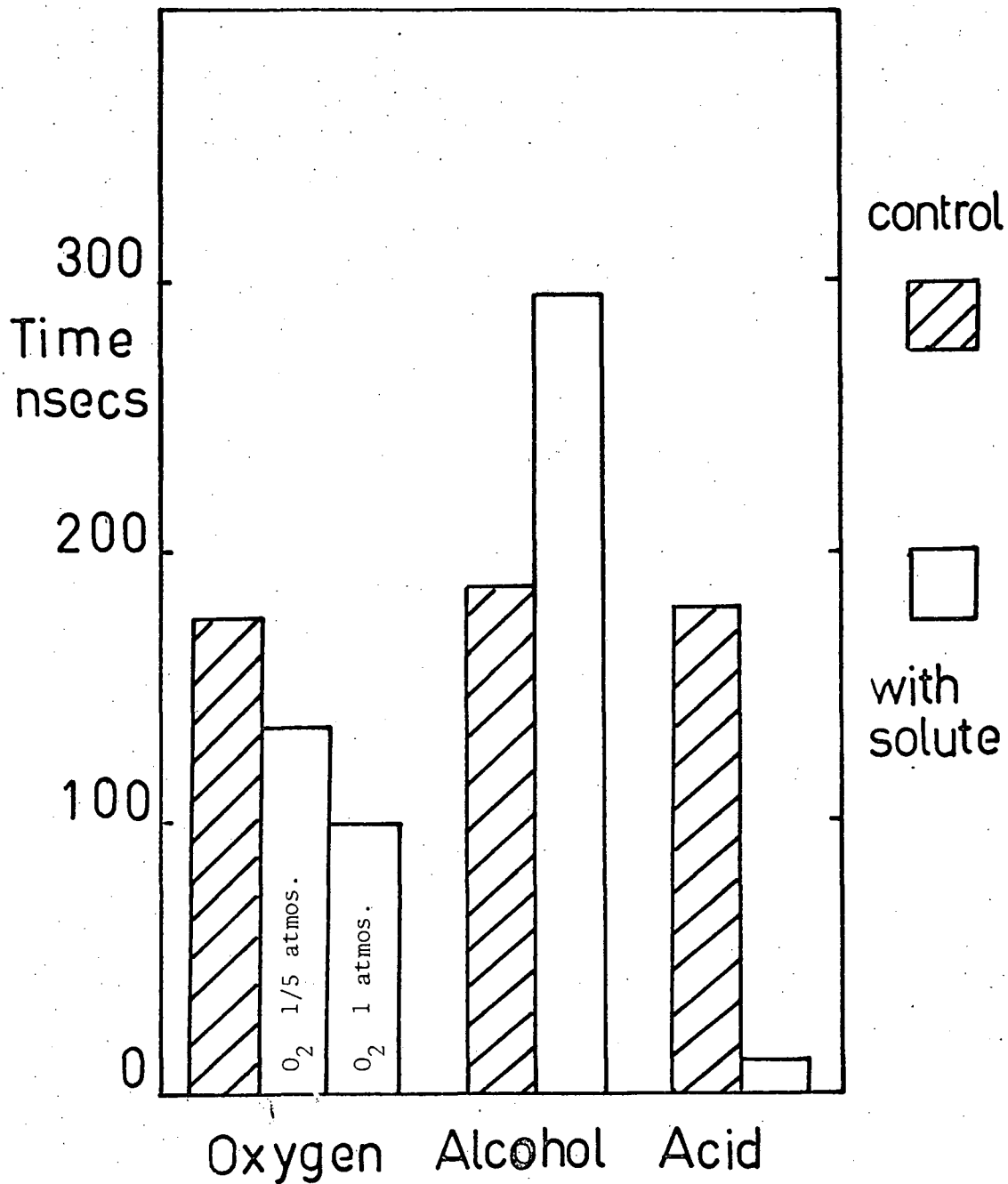
Diagram 18. The time taken for the initial absorption signal of $\bar{e}$ aq to decrease by a factor of 2 in the presence of different solutes.

electron which was to be expected although the curves on the first order

plots had long linear portions to which the computer fitted a rate

constant. Data up to 120 nanoseconds used for the second order plots.

	k_1 sec^{-1}	k_2 M sec^{-1}
Control sample	$8.75 \pm .47 \times 10^6$	$8.43 \pm .25 \times 10^{10}$
atomospheric O_2	$(1.03 \pm .04 \times 10^7)$	$1.12 \pm .25 \times 10^{11}$
saturated O_2	$1.28 \pm .01 \times 10^7$	$1.45 \pm .35 \times 10^{11}$

The effects of these solutes are compared in diagram 18.

The pinhole experiments

In these experiments a study was made of the different initial

optical densities and rate constants observed for the $\bar{e}$ aq decay at

varying positions across the width of the radiation tube. Intuitively

one would expect a higher concentration of reacting species in the

side of the cell through which the electron beam first penetrates as

it is here that the majority of secondary ionisations will occur. The

pinhole restrictor plate has already been described and trial experiments

indicated that pinhole no. 2 (0.0225 thou') was the most satisfactory

compromise between an adequate intensity for the emerging laser beam

and the ratio of the diameter of the pinhole to that of the beam. The

positions were recorded as near, centre and far (see diagram 19). Great

care was taken to scan only the main portion and avoid the diffracted

and scattered periphery of the laser beam. Attempts to reproduce these

positions on different occasions by visual settings (with the aid of

the fine lateral adjustment on the base of the plate) were reasonably

successful as indicated by the good agreement between the series of

experiments.

The data is tabulated below. In the <u>near</u> position about 86% of the light was initially absorbed, about 66% in <u>centre</u> and only about 43% at the <u>far</u> side. These are average percentages over all experiments and do not vary more than ±5%. The ΔI_{50} is the decrease in the absorption signal after 50 nanoseconds expressed as a percentage of the initial absorption signal; although the latter varies considerably across the tube (indicating a substantial concentration gradient) this value does not. Despite the concentration gradient it appears as though the rate of loss of the absorbing species is not very different across the tube which is perhaps a qualitative statement of first order behaviour.

.

Table IV

Position	Initial O.D.	O.D. at 90 Nsecs.	$\%I_{MAX}$	ΔI_{50}	$k_1 sec^{-1}$	$k_2 M^{-1} sec^{-1}$
NEAR	.89 ± .15	.34	86%	21%	1.01 ± .04 x 10^7	7.02 ±.03 x 10^{10}
CENTRE	.47 ± .06	.23	66%	28%	8.73 ± 1.3 x 10^6	8.03 ± 1.7 x 10^{10}
FAR	.25 ± .04	.16	43%	23%	poor fit	1.36 ± .12 x 10^{11}
WHOLE BEAM	.95	.32	85%	25%	6.10^6	7.10^{10}

A detailed examination of first and second order plots (with points every 5 nanoseconds) of all the data provided no obvious conclusions concerning the kinetic behaviour of $\bar{e}$ aq in these specific areas.

In the <u>near</u> positions the first order plots were consistently good for about 40 nanoseconds after the pulse and then they tailed off;

at approximately the same time the second order plots became linear
and continued so for the remainder of the absorption signal followed,
which was normally 100 nanoseconds. In no instance was the change in
slope a dramatic one. (In taking data from oscilloscope traces every
five nanoseconds one is limited by the duration and noise level on the
trace: on photographs covering several hundred nanoseconds resolution
of less than 10 nanoseconds becomes very uncertain). This appears
to be a real effect, not an artefact due to say some limitation of the
detection system or widely scattered points. The rates given in the
table are averaged over all experiments, and have an absolute value
within framework of the pinhole experiments but are in the first instance
for comparison only with the full beam experiments. The agreement for
the unimolecular (now refered to as k_1) and bimolecular (now referred
to as k_2) rate constants were good, and both k_1 and k_2 represent very
fast reactions. Treatment (i) did not give any useful results.

In the centre position the graphs were almost as well matched
as those of the near positions but it was more difficult to judge the
slopes. It did not appear that two mechanisms were occurring simultaneously
as treatment (i) gave very poor results. The only clear fact was that
the data could fit both first and second order treatments quite adequately,
and this in itself was confusing. A subtle change in slope appeared
in some of second order plots indicating linearity above $\sim$35 nanoseconds
(after the pulse) when the initial absorption signal had decreased by
some 15%, but to what extent if any this is a change in slope is due
to a change in mechanism is open to speculation. The first order plots

ΔOD = (OD$_{t=0}$ − OD$_{t=90}$)

Diagram 19. The first order decay of ē aq in the pinhole experiments.
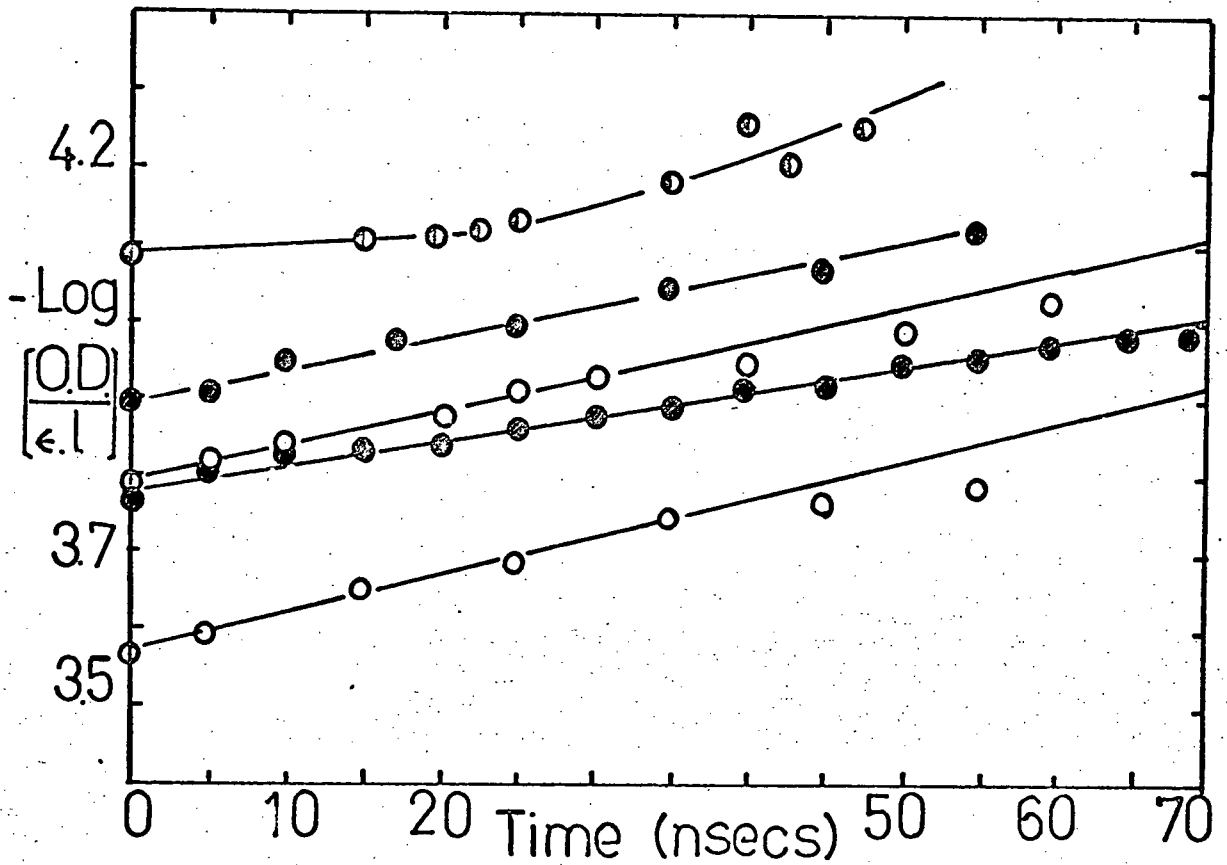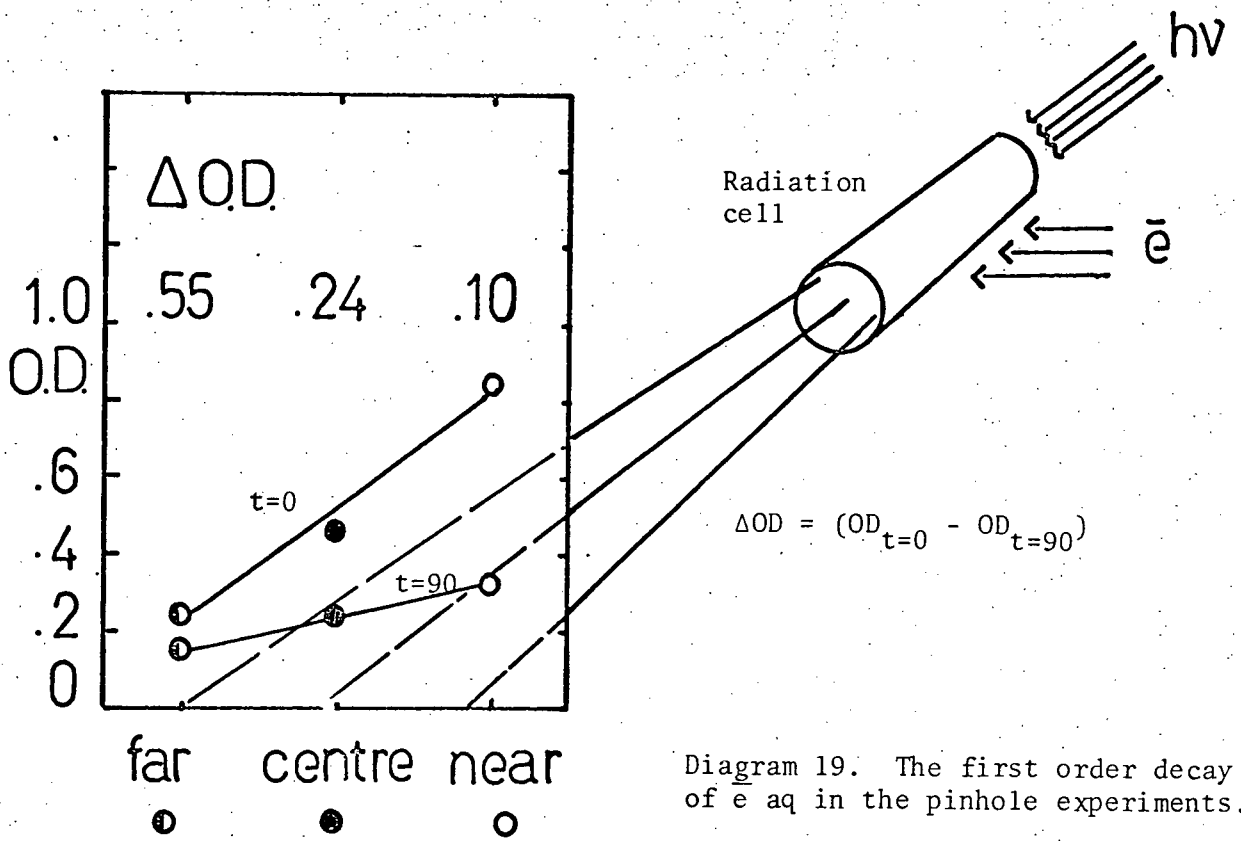
were linear as far as they were followed, to 65 nanoseconds; the reasons for this seemingly short data-period have already been given. The k_1 and k_2 evaluated from these slopes (k_2 after 35 nanoseconds) are again high but although the average values are slightly lower than the k_1, k_2 (near), individual values are in the same range, and within experimental error can be considered constant.

Finally the data from the far position was compared to that discussed above and this time graphical analysis indicated rather poor first order and reasonable second order fits. Treatment (i) was uninformative here too. However another curious feature appeared in the absorption and decay signals of most of these experiments. The initial 25 ± 5 nanoseconds were characterised by a plateau after which the decay of the absorbing specie was bimolecular. In view of the relatively weak absorption observed in the far position and thus the poor signal to noise ratio it is not at present possible to decide unequivocally whether the plateau was in fact an extremely slow decay whose slope could not be determined at the levels of sensitivity employed, or whether it represented a time "equilibrium" in that far region of the radiation cell. Again it is felt that this is a genuine result and not a technical artefact as it was reproducible on different occasions when the components of the detection and monitoring system were individually checked. The second order rate constant for the disappearance of the absorbing specie was determined to be $1.36 \pm .12 \times 10^{11}$ which is significantly faster than the other k_2 values.

In summary the pinhole experiments lead to three conclusions. First that there is a marked change in optical density across the depth

of the irradiated volume of liquid which in terms of the concentration

of the hydrated electron means about a 70% decrease from 2.9×10^{-4} M

at the <u>near</u> edge to 8×10^{-5} M at the <u>far</u> edge. Secondly the kinetics are

complex even in the restricted regions of the irradiation liquid that

were studied; only in the <u>far</u> region do the kinetics appear to be second

order, while a preference for first order behaviour is indicated else-

where. Thirdly the rate constants are high, k_1 being of the order 10^7 sec^{-1}

and k_2 varying from 0.70 to 1.36 $\times 10^{10}$ $sec^{-1} M^{-1}$. sec^{-1}

The variations in k_2 will be averaged in a full beam study and

thus illustrate the hazards of making detailed kinetic interpretations

on systems with an inhomogeneous distributions of reacting species.

The deuterated electron

(i) The formation and decay of the deuterated electron were

also studied with the following modifications to the system. A 15 mwatt

spectra physics model 124 Helium Neon laser replaced the 1m watt laser

and the beam emerging from the window of the plexicell was directed on

to the photocathode wires in the photomultiplier tube now out of its

copper housing (and therefore fully exposed to the beam). The aperture

of the iris some 10 cms away from the photomultiplier was adjusted to remove

all the scattered light around the main beam, and all the experiments were

carried out in a darkened room. The lens was omitted from the alignment.

The very high frequency signals observed from the 1 m watt laser were

not unexpectedly present (in view of their probable origin) in this more

powerful laser, but operating the photomultiplier at 500 volts gave a

S:N ratio of 150:1 under steady state conditions and about 25:1 during and

immediately after the electron pulse. The photomultiplier was not saturated by the light intensity (although the concept of shining such a laser at a photomultiplier is not to be too readily accepted) under the working conditions. The apparent improvement in the S:N ratio can be attributed to the lower working voltage on the photomultiplier and the increase in available light intensity which permitted a higher attenuation to be used in recording the signals.

(ii) Unfortunately the limited supply of D_2O immediately available was insufficient for degassing to take place in the manner previously described. A 50 ml sample of D_2O (Merck.S&D.) in a sealed, sterilised polythene container was vigorously degassed with helium supplied through a frittered glass oval and escaping via a temporary opening. After thirty minutes of shaking and degassing the gas-line on the container was quickly exchanged for a short fitted nozzle. The latter slipped into the filling part of the plexicell and thus the D_2O was introduced by pressurising the container. When the cell was full and there were no gas bubbles present the nozzle was removed and both parts sealed.

The oxygen content of the D_2O was certainly less than atmospheric but greater than that estimated for the liquid water experiments. The effect of oxygen on the decay of $\overline{e}$ aq has been studied and from this it is felt that the probable amount of oxygen present would not greatly effect the observed rate constants for the decay of $\overline{e}_d$, but nevertheless more accurate determinations can be made. The pinhole experiment was repeated with D_2O, but here the presence of oxygen and radiation products owing to the necessity of repetitive pulsing in many instances permits only a
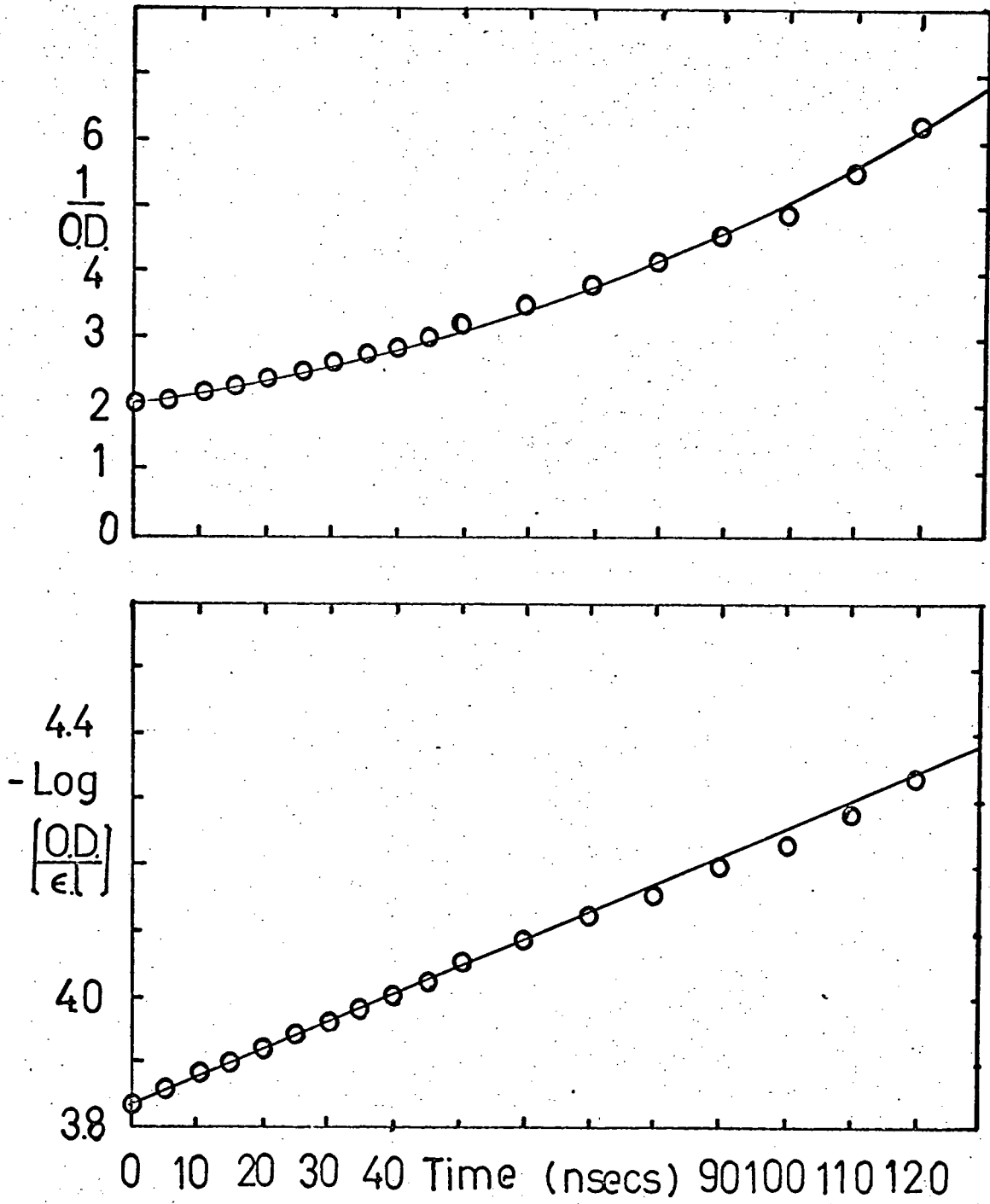
Diagram 15 (a). The decay of the deuterated electron

qualitative statement of the results.

(iii) The decay of $\bar{e}_d$ was undoubtedly first order for the initial 90 nanoseconds after the pulse using the full beam but the deviation from the linear plot was not very pronounced even at 120 nanoseconds; second order treatment gave no satisfactory fits although an approximate estimate of the bimolecular rate constant was 10^{11} M^{-1} sec^{-1} as the fit improved. The decay of $\bar{e}_d$ after 2 consecutive pulses essentially followed second order kinetics. In neither case did treatment (i) indicate two simultaneously occurring processes.

The pinhole experiments again showed a marked concentration gradient across the depth of the irradiated volume but no attempt will be made to differentiate between the processes occurring in the different areas for reasons given above. The ΔI_{50} values varied little in these areas, but curiously decreased after two pulses. This may be an artefact. A few comparisons are made below. A path length of 0.25 mm was used.

Table V

Region	O.D.	ΔI_{50}	k_1 sec^{-1}	k_2 M^{-1} sec^{-1}
Full beam 1 pulse	.67 ±.16	30%	$8.14 \pm .21 \times 10^6$	(10^{11})*
Full beam 2 pulses	.67 ±.16	20%	(10^7)	$9.88 \pm .50 \times 10^{10}$
NEAR	It = 0	14%	(10^6)	(3.10^{10})
CENTRE	1.8 ± .1	13%	(10^6)	(4.10^{10})
FAR	.77 ± .06	11%	poor fit	(6.10^{10})

*the data in brackets are only included to show the relative rates that were indicated and imply nothing more.

In summary the decay of the deuterated electron appears to follow first order kinetics for about 90 nanoseconds after the pulse and then tends towards second order behaviour as was observed for the hydrated electron.

Interference phenomena

The detection of appreciable fluctuations in high intensity after the electron pulse induced absorption, for some while prevented any accurate measurements on the real absorption and decay signal of the hydrated electron. At this stage the plexicell only was being used with no electron beam restrictor block or grounding plate. The fluctuations sometimes amounted to 70% of the initial absorption, were quite reproducible and lasted several microseconds. The possibility that $\bar{e}$ aq* was being photolysed in significant quantities by the high intensity of the laser beam and on returning to the ground state proceeded to absorb once more could not be ruled out. However in experiments under identical conditions but with acidified water (0.1 M H$^+$) the $\bar{e}$ aq absorption completely disappeared as expected but the intensity fluctuations remained as strong and characteristic as in the neutral water experiments. The traces are reproduced in diagram (20) including one showing laser interference. Other possible absorbing species were also ruled out.

Because of the interfering but reproducible nature of these fluctuations a systematic study was made to try and discover their origin and to eliminate them (if not completely) at least from the first 500 nanoseconds on the traces. For convenience these signals will now be called "waves" as this best describes their irregular undulating

No restrictor plate
top: H_2O
bottom: acid
Long pulse

5 mV/div.

200 nsec/div.
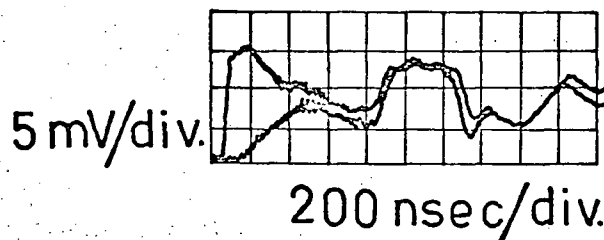
Beam restrictor and Al
block in place
Short pulse – H_2O

10 mV/div.

100 nsec/div.
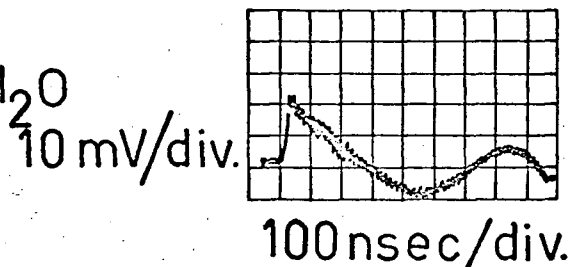
Typical high frequency
laser signal

20 mV/div.

10 nsec/div.
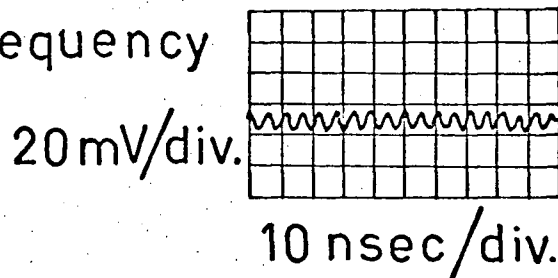
Diagram 20. Oscilloscope traces of the Interference Signals

appearance.

There were three possible general causes for these waves

(i) electrical; ringing in the photomultiplier or reflections in the grounding system, space charge effects, mismatch of transmission lines.

(ii) optical; malfunction of the laser, sudden localised changes in refractive index in the liquid, scattering of light.

(iii) pressure waves; across the irradiation cell after the impact of the electron pulse, shock wave through the air space between the electron tube window and the cell.

The results of the study will be summarised briefly; ultimately it was only possible to delay the onset and reduce the magnitude of the waves, the precise nature of their origin remaining uncertain. In as much as they were not the result of chemical activities of $\bar{e}$ aq and the absorption and decay signals were finally resolved the problem remained a technical one in the context of this research. It would be extremely interesting however to pursue their origin as a primary objective.

(i) electrical: in the absence of the plexicell but otherwise identical conditions the waves could not be observed. Several ground loops were deliberately incorporated to see if the frequency or appearance of the waves could be altered in the presence of the plexicell, but with negative results. The photomultiplier was checked for saturation effects and overshoot; the waves did not reduce or disappear as the photomultiplier operating voltage was increased and therefore space charges as well were ruled out. It appeared that this approach would not lead to the origin of the waves.

(ii) optical: if the laser were switched off (but remained in the circuit) and the acceleration fired under normal experimental conditions the waves disappeared, therefore no emission was contributing to their shape and the valid response of the photomultiplier was confirmed. If the laser was switched on but the plexicell emptied of all solution the waves again were not observed. On substituting a 2 mm diameter glass rod with polished ends for the glass irradiation tube in the cell an absorption signal and permanent change in optical density occurred after 1 μ second (due to the presence of trapped electrons) but the height and shape of the signal indicated that there were no waves superimposed during the initial 500 nanoseconds.

Scattering of the laser beam by dust-particles in solution or microsplinters of glass that may be present in the irradiation tube after several electron pulses was unlikely to cause such enormous fluctuations in the intensity; the waves remained unaffected by changing radiation tubes and using fresh solutions.

The waves therefore were a function of the liquid and it seemed probable that they arose from the sudden localised changes in refractive index that occurred immediately after the pulse along the length of the irradiation tube. The radial distribution of the electron beam itself led to a far higher concentration of electrons in the centre of the irradiation tube in comparison to either end of the tube. However this could not be the complete explanation as the waves continued to appear quite strongly for tens of microseconds after the pulse and any inhomogeneity would be smoothed out within a microsecond.

(iii) pressure waves: the impact of the electron beam is powerful -- in the 2 MeV Febetron 30 nanosecond electron pulse of 1.8 MeV electron shatters any glass windows on the cells and stainless steel must be used (48.). It would not be surprising therefore to have a pressure wave reflecting back and forth across the diameter of the irradiation cell. This pressure wave could arise from the energy transfer between the glass irradition tube and the liquid after the impact of the electron beam, or could be transmitted from a shock wave moving behind the electron beam (as it emerges from the electron-tube window towards the glass tube) across the entire plexicell. Another possibility for an internal pressure wave has been described as 'microcavitation' (49); it is suggested that there is a sudden increase in volume when the electrons finally become solvated (10^{-11} seconds) and this amounts to pocket "explosions" in the liquid.

A pressure wave will give rise to changes in refractive index and thus it is difficult to separate the two ideas experimentally. That there was a significant impact on the radiation tube was shown by filling the plexicell with water containing a very small quantity of oil. The latter settled to the bottom of the tube and did not interfere with the laser beams. On pulsing this solution the same sort of wave signals were recorded with the $\overline{e}$ aq absorption; but projecting the transmitted laser beam on to a screen one could even see the changes in intensity as the oil droplets moved into the path of the beam. The same effect could be produced by gently tapping the tube in the plexicell to mix the liquids.

Other liquids with different viscosities and non H-bonded

solvents were examined in the plexicell and later radiation tubes of up to 1.5 cm in diameter in individual supporting frameworks used to contain these liquids and investigate the properties of the waves at some distance from the formation of the hydrated electron. In these areas the waves were very weak and structureless signals as one might anticipate from a dissipated pressure wave, but in the larger tubes the problem of space charges could no longer be ignored. In solvents of high viscosity the amplitude and frequency of the waves were considerably reduced.

(iv) summary: on the assumption that these waves were phenomenon arising from sudden (internal or external) pressure or concentration changes in the liquid in the cell attempts were made to reduce the air space between the plexicell and the electron-tube window and to collimate the electron beam. The most satisfactory technical arrangements have been described in the experimental section although the beginning of a much weaker wave signal could still be observed after about 600 nanoseconds.

Discussion and Interpretation of the Results

(i)   The behaviour of $\bar{e}$ aq at high dose rates

The aim of this research was to provide a firm basis for the

study of $\bar{e}$ aq* and therefore investigated the decay of $\bar{e}$ aq produced in

high concentrations by an electron pulse, the intensity of which gave

dose rates $\sim 10^2$ above those used in previous investigations.

The disappearance of $\bar{e}$ aq over a period of about 70 to 80

nanoseconds after the 3 nanosecond electron pulse has been shown to follow

a first order decay; there is subsequently a slow transition towards

bimolecular behaviour and this appears to be firmly established in about

100 to 110 nanoseconds after the pulse. It is worth noting that this

transition is contrary to normal classical homogeneous kinetics where a

transition from 2nd → 1st order would be expected as the concentration

of the reactive species decreases. The second-order decay can be followed

for several hundred nanoseconds after the pulse although by this stage

the reactions are not exclusively due to the combination of two hydrated

electrons but generally to reactions with the products of radiolysis.

The pinhole experiments however demonstrated very clearly that

the system was not homogeneous during the first 90 nanoseconds and

that even in localised regions of the irradiated volume the kinetics

are neither first nor second order in the classical sense but are more

complex.

The pattern of behaviour observed for the deuterated electron

followed the same time sequence and again the pinhole experiments demon-

strated that the distribution of absorbing species was inhomogeneous for

a significant interval after the pulse.

The first and second order rate constants evaluated at appropriate times after the pulse are tabulated below together with some second order rate constants published for these reactions.

Table VII.

$$\bar{e}\ aq \longrightarrow ?$$ $$k' = 8.80 \pm .8 \times 10^6 \ sec^{-1}*$$

$$\bar{e}\ aq + \bar{e}\ aq \longrightarrow H_2 + 2OH^-$$ $$k_2 = 5.88 \pm 1.2 \times 10^{10} \ M^{-1} \ sec^{-1*}$$

$$= 1.22 \pm .1 \times 10^{10} \ M^{-1} \ sec^{-1**}$$

$$= 3.2 \times 10^{11} \ M^{-1} \ sec^{-1} \quad (46)$$

$$\bar{e}d \longrightarrow ?$$ $$k'' = 8.14 \pm .21 \times 10^6 \ sec^{-1*}$$

$$\bar{e}d + \bar{e}d \longrightarrow D_2 + 2OD^-$$ $$k_3 = \sim 10^{11} \ M^{-1} sec^{-1*}$$

$$= 1.20 \pm .1 \times 10^{10} \ M^{-1} \ sec^{-1} \quad (30)$$

* this work

**average value from several laboratories: see table II

The bimolecular rate constant determined in this work is a factor of ~ 5 higher than that previously reported and a factor of ~ 5 lower than Klein & Warner's results; a figure approaching their value was estimated for the decay in the far regions of the irradiation tube where the distribution was certainly inhomogeneous and (as later calculations show) would remain so for several hundred nanoseconds. These authors have made the prior assumption of homogeneous kinetics in their system on the basis of the mean lifetime of a spur being $\sim 10^{-8}$ seconds (2). It would appear that the changes in optical density they initially recorded were averages of quite varied changes across their radiation cell due to the inhomogeneous distribution of $\bar{e}\ aq$.

In contrast, the behaviour of $\bar{e}$ aq in the presence of scavenging

species did not show any unpredictable trends. The presence of $\bar{e}$ aq

in the system was confirmed by pulsing an acidified aqueous solution in

which no absorption at 6328 $\overset{o}{A}$ was detected. Under these conditions the

hydrated electron is converted to a hydrogen atom too quickly for $\bar{e}$ aq

to be observed, while at a slightly higher pH the absorption could be

observed very briefly before this conversion was complete. In isopropyl

alcohol solutions the experimental half life (time taken for the initial

absorption signal to fall to half its value) increased as the alcohol

removed H and OH radicals before they could react with $\bar{e}$ aq and deplete

its concentration. The decay was bimolecular although early stages were

ambiguous. The effect of dissolved oxygen in the system was to decrease

the half-life of $\bar{e}$ aq but even inthe oxygen saturated solutions, the

$\bar{e}$ aq would have to move from the spur into the bulk medium before reacting

with the oxygen, as the solute concentration is still only millimolar.

The fundamental problem that has been raised by the events of

the first 100 nanoseconds or so after the electron pulse is one of

inhomogeneity, and one that invalidates the interpretation of the data

from the classical kinetic viewpoint. In order to calculate the time

lapse between the end of the electron pulse and the overlap of the spurs,

that is homogeneous distribution of the hydrated electron, the following

calculations were made.

(ii) A model relating to the distribution of the spurs in space and time

Assume a simple physical model of the irradiated volume of liquid immediately after the pulse, with spurs randomly distributed in small localised areas, but a marked degree of inhomogeneity along the cross section of the volume through which the laser beam is passing. Utilising the data from the pinhole experiments (see Table ^{IV}) the optical density recorded at t = 0 nanoseconds is taken as proportional to the concentration of the absorbing specie in a particular region of the irradiated volume and from this concentration the energy deposited in that region can be estimated. From the latter, the number of spurs is calculable and therefore the mean volume space occupied by a spur. The initial radius of a spur after the pulse is believed to be $\sim$20 $\overset{\circ}{A}$ (12) and if one considers this spur to be centrally located in the mean volume space by regarding the two volumes as concentric spheres then it is possible to determine the distance between the surface of the spur and the limits of the volume in which the spur must be statistically present. The time taken for the spur to diffuse to the limits of the mean volume space is then calculated. As all the spheres representing the mean volume space are in three dimensional contact with neighbouring volumes the time taken for this diffusion is the time lapse before spur overlap creates a homogeneous distribution of hydrated electrons and radicals. The approximations necessary are that the spur is spherical and diffuses with spherical geometry and that the volume of liquid can be represented as an area of close packed spheres in each of which there is unit probability of finding a spur. There is approximately one third free volume space not accounted

for by latter assumption and so this was incorporated into another set of calculations to give an upper limit to the results; the ultimate difference in the time necessary for overlap was not very large, $\sim$10%.

(iii) Calculations and the results

The following constants were used:

$G_{\bar{e} \, aq}$ = 2.6

1 spur = 100 eV

ε = 1.2 x 10^4

ℓ, Path length (for this experiment) 2.6 mm

No = 6.025 x 10^{23}

$D_{\bar{e} \, aq}$ = 4.7 x 10^{-5} cm^2 sec^{-1}

The concentration of $\bar{e}$ aq in a specific region is $\dfrac{OD}{\varepsilon \ell}$

If a deposition of 100 eV gives rise to 2.6 molecules of $\bar{e}$ aq, then the total energy deposited per mL that area is E.

$$E(eVmL^{-1}) = \frac{100 \ eV}{G_{\bar{e} \, aq}} \ . \ \frac{[\bar{e} \ aq]}{10^3} \ . \ No$$

The numbers of spurs, C_s is given by

$$C_s = \frac{E}{100} \quad \text{spurs mL}^{-1}$$

The volume occupied by 1 spur is

$\dfrac{1}{C_s}$ cm^3 $\equiv$ to a sphere of radius r_s.

$$r_s = \left(\frac{3}{4.\pi.C_s} \right)^{1/3} \times 10^8 \ \overset{\circ}{A}$$

A spur has radius r_o at time t_o; the radial difference between the spur and volume of liquid it occupies in this region at t_o is $(r_s - r_o)$.

The time t taken for a spur to diffuse that distance

$$(r_s - r_o) = (Dt)^{1/2}$$

The results of the calculations pertaining to three different areas in the irradiated liquid using data from the pinhole experiments are tabulated below. The upper limit t* on the time is that calculated with the addition of $(\frac{1}{3\bar{C}_s})$ to the mean volume space available. Similar calculations using the optical densities recorded for the whole of the area of the irradiated liquid led to overlap times ranging from 30 to

Table VI

Region	$[\bar{e} \, aq]M$	$C_s \, ml^{-1}$	$r_s \, \overset{\circ}{A}$	t Nsecs	t* Nsecs
NEAR	2.85×10^{-4}	6.57×10^{16}	153	39	43
CENTRE	1.50×10^{-4}	3.46×10^{16}	190	62	76
FAR	8.0×10^{-5}	1.84×10^{16}	558	503	538

90 nanoseconds. However in these instances one is working at an average situation and the time taken for the actual distribution of the spurs to be truly homogeneous may be quite different. The results of the calculations are shown pictorially in diagram 21.

These calculations show that about 50% of the energy deposited in spurs (not all the energy is transferred to the medium via spurs) may be found within a very localised region where the electron pulse first penetrates, some 30% at a greater distance away and about 1.5 mm away from the dominant site of ionisation and excitation about 15%. These are only general figures but the last one may explain the appearance of a plateau on the absorption and decay traces taken in the far region of the tube. The spurs here are so isolated that the $\bar{e}$ aq cannot react
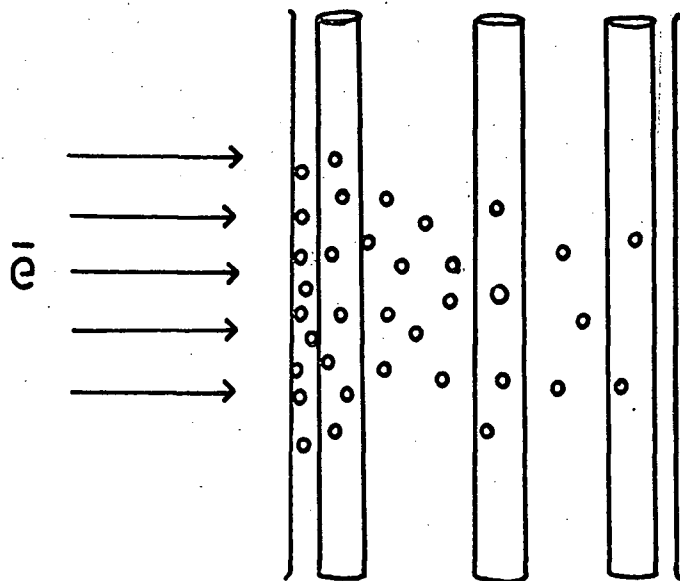
normalised distribution of
spurs (immediately after the
electron pulse) in the laser
beam.
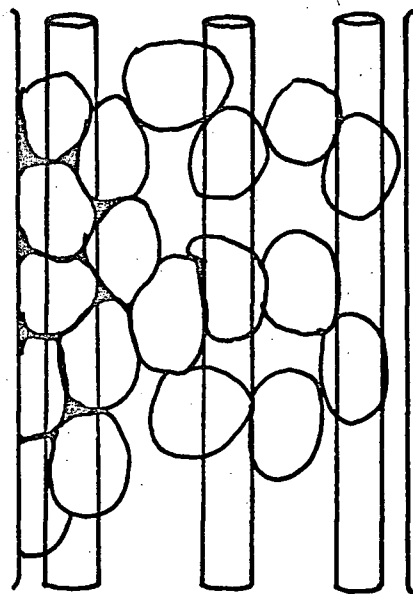
Diffusion of spurs into bulk
volume in 40 nanoseconds still
leaves regions of inhomogeneity
at far side of radiation cell.

near · centre · far

Diagram 21. Pictoral Representation of the spur overlap
calculations.

except (assuming the bimolecular decay with itself) with another $\bar{e}$ aq

or radical in the same spur. As the spur is diffusing in time the

probability of intra spur reaction steadily decreases, although the

random distribution of spurs may give rise to a greater extent of

reaction than is predicted by assuming regular interspur distances.

It was stated in part III that detailed graphical analysis

showed consistently good first order plots for the decay of $\bar{e}$ aq in the

near region up to 40 nanoseconds and after that time the second order

plots became linear within the margin of experimental error. Even fortuitous

results are encouraging as the time calculated for the spurs to overlap

in this region was 39 to 43 Nsecs. The data had been scrutinised and

tabulated before these calculations were performed and it was stated that

the first order decay for the centre position was linear up to 65 nanoseconds

the length of the data period. In the light of these calculations the

spurs were in the process of overlapping at this time; thus it would not

be possible to see a definite change in slope as insufficient data

was available. The "subtle change" in the slope around 35 nanoseconds

is still open to speculation.

Similarly it is not surprising that the graphs from the far

region were slightly different in relation to these others, and the

very fast bimolecular rate constant ($>10^{11}$ M^{-1} sec^{-1}) must be considered

to be an unrealistic evaluation because in converting optical density

to concentration homogeneity has been assumed.

In conclusion these calculations (in spite of the reasonable

arguments against the approximations but the lack of equally reasonable

alternatives) appear to be qualitatively successful in explaining the inhomogeneity observed in regions of the irradiated volume and in providing an acceptable basis for the change in slope that appears in all the first order plots for the decay of the hydrated electron.

(iv) The bimolecular decay

A rate constant of $(5.88 \pm 1.)10^{10}$ $M^{-1}sec^{-1}$ has been determined for a second order decay after the initial 50 nanoseconds . There will be significant amounts of other radicals and ions at this stage and so the decay will not be solely due to

$$\overline{e} \text{ aq} + \overline{e} \text{ aq} \xrightarrow{k_1} H_2 + 2OH^- \quad k_1 = 9.10^9 \text{ } M^{-1} \text{ sec}^{-1}$$

but will also include

$$\overline{e} \text{ aq} + OH \xrightarrow{k_2} OH^- \text{ aq} \quad k_2 = 3.10^{10} \text{ } M^{-1} \text{ sec}^{-1}$$

$$\overline{e} \text{ aq} + H_3O^+ \xrightarrow{k_3} H + OH^- \quad k_3 = 2.32.10^{10} \text{ } M^{-1} \text{ sec}^{-1}$$
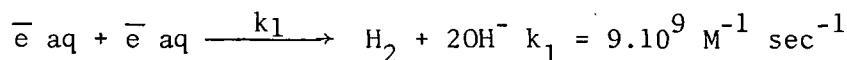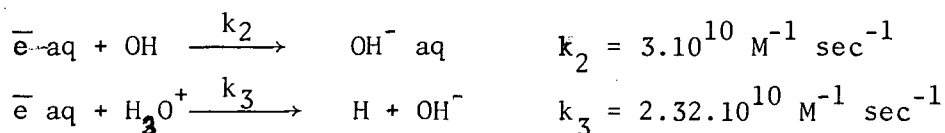
and contributions from OH will decrease rapidly due to

$$OH + OH \xrightarrow{k_4} H_2O_2 \quad k_4 = 4 \times 10^9 \text{ } M^{-1} \text{ sec}^{-1}$$

As the G-values for all these other species are approximately the same one can assume that their initial concentrations are the same and the expression for the loss of $\overline{e}$ aq

$$\frac{-d(\overline{e} \text{ aq})}{dt} = k_1[\overline{e} \text{ aq}]^2 + k_2[\overline{e} \text{ aq}][OH] + k_3[\overline{e} \text{ aq}][H_3O^+]$$

can be simplified to

$$= (k_1 + k_2 + k_3)[\overline{e} \text{ aq}]^2$$

By adding the values for the rate constants one has a composite rate constant for the bimolecular decay of $6.2.10^{10}$ M^{-1} sec^{-1} and the averaging experimentally determined value of $5.88.10^{10}$ M^{-1} sec^{-1} is in good agreement.

Alhtough not as much information is available for $\overline{e}_d$, the same explanation can be offered to explain the bimolecular rate constant to $\sim 10^{11}$ M^{-1} sec^{-1} as in all of its reactions studied (except for $\overline{e}_d + D_2O$) $\overline{e}_d$ has rate constants very similar to $\overline{e}$ aq.

(v) First order decay

      Although the kinetic situation is far from ideal, there must
be more than a casual sequence of events that gives rise to the consis-
tently observed first order decay. And if there were the events would
be taking place in the spurs themselves which immediately transfers the
situation into an environment about which little is known and much is
discussed. (Even the second order process might be the overall picture
of two first order processes though against all published work this is
doubtful).

      Therefore two possible mechanisms that could give rise to
first order decay in the classical sense will be outlined briefly.

      The time calculated for overlap is an average parameter
because in the real case there may at any time be a significant number
of spurs overlapping due to the partition of the energy of the primary
incident electron into blobs, short tracks and spurs. For a 0.5 MeV
electron about 64% of the primary energy finds itself in isolated spurs
but there are substantial contributions from blobs (12%) and short tracks
(24%). The chemical effects that take place in these areas occur in
isolation although, for example, at the end of a cylindrical track
there may be quite a high local concentration of radical species.
These species are still temporarily isolated from the other events
occurring in the medium, and may react with each other within the
spur. The radical species thus distributed in the liquid after
the electron pulse may diffuse together to form 'encounter-pairs',
a transient intermediate whose occurrence depends on the proximity of

the species and the encounter time. The rate of disappearance of this species depends on two factors; these are (i) the frequency of pair encounter within the spur and (ii) the number of pairs, therefore the number of spurs in the path of the laser beam. This probability of an event taking place would give rise to an overall first order.

Suppose for instance that there were a certain probability of two hydrated electrons forming such a transient intermediate which could either relax into the free species again or react quickly to give the familiar radiolytic products. In the latter case the concentration of the hydrated electron would be decreasing at a rate proportional to the rate of formation of the intermediate. Perhaps $\bar{e}$ aq + $\bar{e}$ aq $\underset{k_{-1}}{\overset{k_1}{\rightleftharpoons}}$ $(e)_2^{2-}$ aq is established and the probability of further reaction in the spur is zero order;

$$(e)_2^{2-} aq \xrightarrow{k_2} H_2 + 2OH^- aq$$
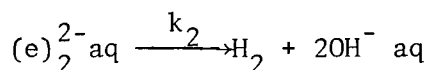
or, if the encounter-pair relaxes to give two hydrated electrons,

$$2\bar{e} \, aq \longrightarrow H_2 + 2OH^- \, aq.$$
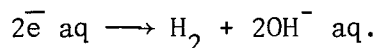
But as the number of spurs is reflected in the optical density measurements, the rate of loss of $\bar{e}$ aq as measured experimentally by $\frac{\Delta OD}{dt}$ will give rise to a first order decay.

The diminishing concentration of $\bar{e}$ aq and the rapidly expanding spur (due to the diffusion of species within the spur) limit the time up to which these intraspur encounters have any significance. When the spurs have overlapped then the dominant decay is through interspur mechanisms. If an equilibrium between $\bar{e}$ aq and the $(e)_2^{2-}$ aq did exist then the k_{-1} term may be large enough to observe a true equilibrium experimentally when the number of encounter pairs (or spurs) is relatively small, and

this is possibly another reason behind the plateau observed in the far region in the pinhole experiments.

There are many considerations to an approach of this kind the Thermodynamics of the reaction sequence and the magnitude of the force fields in the liquid (which can produce appreciable changes in the structure in the liquid) being two of basic importance.

Whereas above the formation of an encounter-pair was proposed, an alternative is the rapid formation in the spur of a correlated ion-pair,

$$\overline{e} \text{ aq} + H_3O^+ \longrightarrow H_3O^+ \overline{e} \text{ aq}$$

$$H_3O^+.\overline{e} \text{ aq} \longrightarrow H_2O + H$$
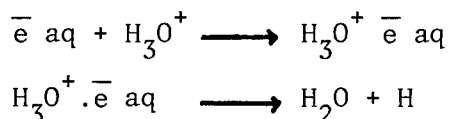
which then breaks up to give a hydrogen atom and water. If the only reason for the decay of the species in the spur is through such a mechanism (analogous to electron-hole pairs) then the separation and coulombic attractions between the ions is of critical importance. The ion in diffusing away from its origin will see a time dependent coulombic field due to the spatial distribution of the other ions in the spur, and if this energy is comparable to thermal energies it is unlikely such ion pair combinations could occur. [Similar monomer and dimer species that are essentially ion-pairs have been postulated for electrons in ammonia (50)]. The controversies associated with the recapture of electrons are fundamental problems in this field of study (10,11).

Work published on the recombination of trapped electrons in glasses and frozen matrices has also shown first order decay behaviour and suggestions have been made that the disappearance of the electron is through geminate recombination with the positive ions (14). According

to the distribution of the ions both first and second order decays

could be observed and the recombination times were markedly temperature

dependent. Similar work (42,43) showed a temperature dependent first order

going into overall second order decay in glasses as the temperature rose

and the electrons became free to diffuse. This was taken as evidence for

different kind of traps.

Recently (51) the electron-hole pair has again been discussed

in terms of an exciton viz $[(H_2O)^+ \cdots (H_2O)^-]$, two of which ultimately

give rise to molecular products of hydrogen, water and hydrogen peroxide.

Although the proposal in the main relates to experimental results in ice,

Weiss regards the situation in pulse radiolysed water in the nanosecond

region as analogous.

(vi) Epilogue

As a basis for study on the nature of $\overline{e}^*$ aq this work provided

some unexpected but not surprising conclusions relating to the inhomo-

geneous distribution of the species whose kinetic behaviour was under

investigation. If the initial decay mechanism is a real first order

process the precise sequence of events is open to speculation although

an equilibrium or charge correlation model might be considered. The

bimolecular rate constant determined was a factor of 5 lower than Klein

and Warner's result despite the 10^2 increase in the dose rate. The inhomo-

geneity of the system adds some uncertainty to even this determination

and undoubtedly accounts for their high value. It is apparent that in

studying reactions occurring in tens of nanoseconds one cannot justifiably

convert optical densities into concentrations on which the bimolecular

rate constants depend. Because of the existence of localised areas of

very high concentrations of reactive species the Beer-Lambert relationship which applies to homogeneous and continuous systems breaks down. Nevertheless the initial mode of behaviour and half life of $\overline{e}$ aq in our system in the absence of any photolysing light has been established and the next experiments will be to look at the behaviour of $\overline{e}^*$ aq by flashing photolysing the hydrated electron.

References

1. I.V. Vereshchinskii & A.K. Pikaev, Introduction to Radiation Chemistry, English translation from Isreal Program for Scientific translations, Jerusalem (1964).

2. J.W.T. Spinks & R.J. Woods, An Introduction to Radiation Chemistry, John Wiley & Sons, N.Y. (1964).

3. A.E. Moelwyn-Hughes, Physical Chemistry, Pergamon Press, Oxford (1961)

4. R.F. Gould (Editor) Solvated Electron, Am. Chem. Soc. Publication, Washington (1965).

5. D.C. Walker, in press.

6. A Mozumder & J.L. Magee, Rad. Res., 28, 203-214, (1964).

7. A. Mozumder & J.L. Magee, Rad. Res., 28, 215-231 (1964).

8. A.H. Samuel & J.L. Magee, J. Chem. Phys., 21, 1080 (1953).

9. R.L. Platzman, Physical & Chemical Aspects of Basic Mechanisms in Radiobiology, Pub. no. 305, 22 (U.S./NRC) (1953).

10. L.H. Gray, J. Chim. Phys. 48, 172 (1951).

11. J.L. Magee. Proc. Inf. Conf., Highland Park Illinois N.A.S., 305, 22 (1953).

12. A. Kupperman, Diffusion Kinetics in Radiation Chemistry.

13. E.A. Shaede, M.Sc. Thesis (1967).

14. Proc. Vth Inf. Conf. on the Radiation Chemistry of water AEC no COO-38-519.

15. J. Boag & E.J. Hart, Nature, 197, 45 (1963).

16. E.J. Hart & J. Boag, J.A.C.S. 84, 4090 (1962).

17. J. Weiss, Nature, 153, 748 (1944).

18. R.L. Platzman, Proc. Inf. Conf., Highland Park Illinois, N.A.S. 305, 22 (1953).

19. G. Stein, Disc. Farad. Soc., 12, 227 (1952).

20. E.J. Hart, J.A.C.S., 76, 4312 (1954).

21. E. Hayon & J. Weiss. Proc. Intern. Conf. of Peaceful uses of Atomic Energy (2) <u>29</u>, 80 (1952).

22. N.F. Barr & A.D. Allen, J. Phys. Chem., <u>63</u>, 628 (1959).

23. J.H. Baxendale & G. Hughes, Z. Phys. Chem. (Frankfurt) <u>14</u>, 306, (1958).

24. G. Czapski & H.A. Schwarz, J. Phys. Chem., <u>66</u>, 471 (1962).

25. E. Collinson, F.S. Dainton, D.R. Smith & S. Tazuke, Proc. Chem. Soc. 140 (1962).

26. F.S. Dainton & W.S. Watt, Proc. Roy. Soc. <u>275A</u>, 447 (1963).

27. J.P. Keene, Nature <u>197</u>, 47 (1963).

28. M.S. Matheson, Ann. Rev. Phys. Chem. <u>13</u>, 77 (1962).

29. M. Anbar & P. Neta, Int. J. of App. Rad. & Isotopes <u>18</u>, 493 (1967).

30. E.J. Hart & E.M. Fielden, J. Phys. Chem. <u>72</u>, 577 (1968).

31. R. Schiller, J. Chem. Phys. <u>47</u>, 2278 (1967).
32.   Ibid   2281 (1967).

33. G.R. Freeman & J.M. Fayadh, J. Chem. Phys. <u>43</u> 86 (1965).

34. J.E. Bennet, B. Mile & A. Thomas, J. Chem. Soc. A 1967, 1394.

35. V.N. Shubin, V.A. Zhigunov, V.I. Zolotarevsky & P.I. Dolin , Nature <u>212</u>, 1002 (1966).

36. L.M. Dorfman (ed. R. Gould), <u>Solvated Electron</u>, opus cit.

37. J. Jortner, Rad. Res. Suppl. no. 4, 24-34 (1964).

38. W.C. Gottschall & E.J. Hart, J. Phys. Chem. <u>71</u>, 2102 (1967).

39. R.L. Potter, R.G. Shares & J.L. Dye, J. Chem. Phys. <u>35</u>, 1907 (1961).

40. J.H. Baxendate, Rad. Res. Supple. no. 4, 139 (1964).

41. D.C. Walker, Quart. Rev. Chem. Soc. 1967 (XXI no. 1.

42. F.S. Dainton, G.A. Salmar & J. Teple, Proc. Roy. Soc. (1965) <u>286A</u>, 27.

43. Ibid, 319.

44. D. Schulte-Frohlinde & K. Eiben, Z. Natur-forsch. 17a, 445 (1962).

45. N. Klein & J. Warner, U.S. Army Nucl. Def. Lab., Doc AD634693 (1965).

46. M. S. Matheson & J. Rabani, J. Phys. Chem. 69, 1324 (1965).

47. L.M. Dorfman & I.A. Taub, J.A.C.S., 85, 2370 (1963).

48. A.W. Boyd, Personal communication.

49. L.M. Dorfman, Personal communication.

50. W. Jolly, N.A.T.O. Adv. Study, Inst. (Hamilton, Ontario) 1967 (see also reference 4)

51. J.J. Weiss, Nature, 215, 151 (1967).

References 1 - 4 were used for general background information.

Corrections

Page	Line	Correction
16	12	include ref. (9) after Platzman
97	ref. 12	A. Kupperman (ed. M. Haissinsky). The Chemical & Biological Action of Radiations, vol. V Publ. Academic Press 1961.
98	ref. 40	J.H. Baxendale.....
98	ref. 42	.....G.A. Salmon.....